Spatial variability of the winter thermal inversion in the northern Bay of Bengal

Md Masud-Ul-Alam (M.S.) [a,b,*], Md. Ashif Imam Khan (B.Sc.) [a], Bradford S. Barrett (Ph.D.) [c], Sara Rivero-Calle (Ph.D.) [b], Md Rony Golder (M.Sc.) [d], Muhammad Abdur Rouf (Ph.D.) [d]

[a] *Department of Oceanography and Hydrography, Bangabandhu Sheikh Mujibur Rahman Maritime University, Dhaka 1216, Bangladesh*
[b] *Department of Marine Sciences, Skidaway Institute of Oceanography, The University of Georgia, 10 Ocean Science Circle, Savannah, 31411, GA, USA*
[c] *Air Force Office of Scientific Research (AFOSR), 875 North Randolph Street, Arlington, VA 22203-1768, USA*
[d] *Fisheries and Marine Resource Technology Discipline, Khulna University, Khulna-9208, Bangladesh*

ABSTRACT

The thermal inversion (TI) is an interesting feature of the global ocean that plays a significant role in ocean-atmospheric process. This study addressed the spatial variability of the TI in the northern Bay of Bengal (NBoB) associated with mixed layer depth (MLD), isothermal layer depth (ILD), barrier layer thickness (BLT), and water mass formation in the winter season. Temperature, salinity, and density measurements were obtained via Conductivity, Temperature, Depth (CTD) casts from 12 different stations. The stations were divided into two regions: the north-western BoB (NW-BoB, 89.5°E: 90.5°E; 21.1°N to 21.6°N), and the north-eastern BoB (NE-BoB, 91°E to 92.1°E; 20.5°N to 21.2°N). Average profiles of the NW-BoB had deeper mixed layer (MLD of 10.30 m) and isothermal layer (ILD of 8.40 m) than profiles in the NE-BoB. The barrier layer in the NW-BoB was also thicker (2.79 m) than in the NE-BoB (1.05 m). One possible reason for these differences is the massive freshwater influx in the NW-BoB, as freshwater reduces salinity (27 PSU in the NW-BoB versus 35 PSU in the NE-BoB) and results in shallower MLD and ILD. Spatially organized TIs occurred in both the NE-BoB and NW-BoB during winter (January–February). Two distinct TI layers at 5 m and 28 m depth were visible in the NE-BoB to the formation of two water masses, the Bay of Bengal Low Salinity Water Mass and the Preparis Channel Water Mass. The NW-BoB featured only one TI layer at 8 m (with a inversion temperature of 0.58 °C), which was associated with the formation of one distinct water mass, the Bay of Bengal Intermediate Water Mass. Spatial variability of the TIs is a function of freshwater flux and surface cooling in the NBoB. More detailed investigation is needed to further understand the TIs and in the NBoB.

1. Introduction

The tropical seas are the hottest regions in the global ocean, where the vertical profile of temperature typically shows upper-ocean water with almost uniform temperature followed by a decrease in temperature with increasing depth (Fig. 1a). This uniform upper-ocean temperature usually represents a layer where the physical properties such as temperature, salinity, and density are well mixed. However, this is not always true for every region in the global tropics. There are several regions in the tropical oceans where the temperature of the upper ocean shows an increase with increasing depth (called a thermal inversion hereafter) instead of a decrease (Fig. 1b). This usually occurs in regions where the freshwater flux (evaporation (E) minus precipitation (P), E-P) is negative and/or the region receives significant volumes of freshwater through river runoff. In general, equatorial regions show a negative freshwater flux (but not all of them exhibit thermal inversions), as precipitation is greater than evaporation. Therefore, the necessary condition for the formation of TI is the presence of sufficiently thick low-salinity layer in the upper ocean that undergoes strong seasonal warming and cooling. The Bay of Bengal (BoB) is one such region where the above conditions required to form TI are satisfied.

The thermal inversion is a prominent aspect of the tropical ocean, as it is widely documented in low to mid-latitude regions (Siddique et al., 2021). TIs occur when surface and subsurface colder water contains relatively warmer water that is sandwiched

* Corresponding author at: Department of Marine Sciences, Skidaway Institute of Oceanography, The University of Georgia, 10 Ocean Science Circle, Savannah, 31411, GA, USA.

E-mail addresses: masudocndu@uga.edu, masud.ocn@bsmrmu.edu.bd (M. Masud-Ul-Alam), ashif.ik.1447@gmail.com (M.A.I. Khan), bradford.barrett@us.af.mil (B.S. Barrett), rivero@uga.edu (S. Rivero-Calle), ronygolderku@gmail.com (M.R. Golder), roufku@yahoo.com (M.A. Rouf).
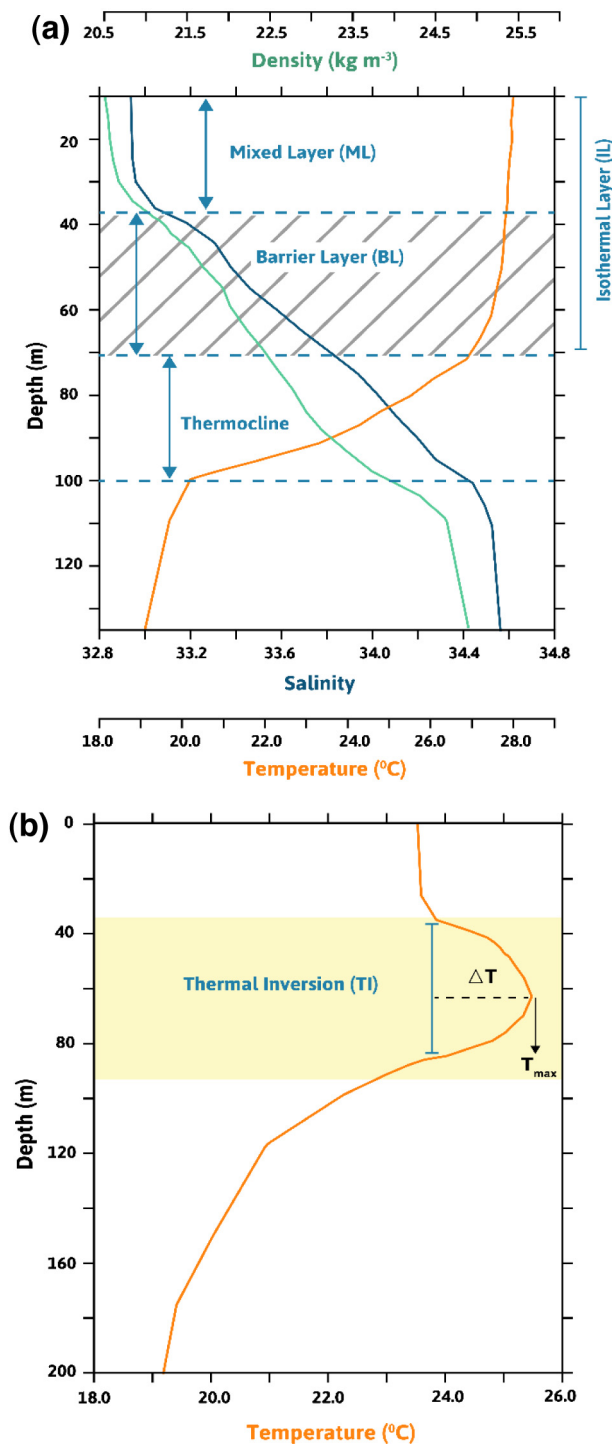
Fig. 1. (a) Schematic diagram showing general configuration of temperature, salinity, and density profiles in the tropics. Mixed, Barrier, and Isothermal Layers are labeled at their corresponding depths. (b) Thermal inversion in a schematic temperature profiles. ΔT indicates temperature difference while the maximum temperature is noted by T_{max}.

between them. This trait is usually identified at a depth in vertical profiles of temperature, where the ocean temperature is warmer than the sea surface temperature (SST) by at least 0.1 °C (Thadathil et al., 2016). TIs can also occur when water masses with contrasting physical properties encounter each other (Kim et al., 2020). The exsisting water masses in the BoB have been previously reported by several researchers (Kumar and Li, 1996;

Rao et al., 1996; You, 2000, 1997). Two noteworthy water masses consists of the warm, high-salinity water mass at relatively shallow depths (40–100 m), which originates from the Arabian Sea. During the southwest monsoon, this water mass intrudes up to 14°N, in the southwestern and central BoB (Murty et al., 1992). In contrast, freshwater input from the surrounding rivers, forms the low-salinity water mass (Shenoi et al., 2002). Sardessai et al. (2007) mentioned the presence of a BoB subsurface water mass (∼35 PSU), ranging from depths between 100 m and 300 m. Based on potential temperature–salinity correlations, Sengupta et al. (2013) described three different water masses in the BoB (Murty et al., 1992; Tomczak and Godfrey, 2003). The first one is situated from 80 m to 100 m, known as the BoB Water mass (34.5 PSU). The second is the Australasian Mediterranean Water, also known as the Indonesian throughflow (ITF, 28.8 °C). Originating from the Pacific Ocean Central Water, this water mass (100 m–500 m) actually forms while passing through the Indonesian Seas (Nyadjro et al., 2010; Potemra, 2005). Lastly, the third water mass is found between ITF and its lower adjacent water mass, called Indian Ocean Deep Water (IDW). It is Antarctic Bottom Water's north moving advected extension (Clowes and Deacon, 1935). In another study, Singh et al. (2012) stated that there could be up to nine water masses (Table 2) that are present in the BoB region.

Many studies were done on the TIs in the global ocean (open waters and continental shelf region), only a few (none) of them were in the BoB (continental shelf of the BoB). The northern Pacific Ocean goes through temperature inversions that are closely associated with the northern sub-tropical Pacific's intermediate water (Ueno and Yasuda, 2003). Near-surface TI, although varying in magnitude of the temperature reversal, is also present year-round in the East China Sea's Shelf (Chen et al., 2019; Yuan et al., 2010). The south-eastern Arabian Sea mostly presents a stable TI during December to February (in winter) because warm, high-saline water gets overlaid by advection of cooler low-saline water (Shankar et al., 2004; Thadathil and Gosh, 1992). Additionally, from November to February, the Lakshadweep Sea (at the southern tip of India) features a westward propagating TI (Durand, 2004; Shankar, 2004) near the surface, which coincides with the low-saline water intrusion from the BoB (Kurian and Vinayachandran, 2006). TIs are also evident in the eastern and central Equatorial Indian Ocean during April–November (Thompson et al., 2006).

The Indian Ocean (IO) in the tropics is bounded by the Eurasian landmass to the North; this distinctive geographical condition gives rise to remarkable seasonality. The IO is predominantly affected by seasonal monsoon winds that reverse twice a year. From May to September, the surface wind blows from the southwest (SW) direction, and between November and February, the surface wind blows from the north-east (NE) direction (Vinayachandran et al., 1996). The BoB, the northeastern part of the IO (Fig. 2), and one of the largest bays in the world with a semi-enclosed basin and is no exception to seasonally reversing winds. The focus of this study, the northern Bay of Bengal (NBoB), is heavily influenced by immense freshwater influxes from the north (Masud-Ul-Alam et al., 2020b,a), making it more vertically stratified than its southern counterpart (Vinayachandran et al., 2002). Simultaneously with this seasonal freshwater influx, there is a freshwater input of 1.625×10^{12} m³ year⁻¹ (Subramanian, 1993) from nearby rivers results in excess precipitation over evaporation (∼2 m year⁻¹, Prasad (1997)). Such a massive amount of freshwater input results in the formation of a "barrier layer" possessing a strong halocline in the upper isothermal layer depth (ILD) (Lukas and Lindstrom, 1991; Sprintall and Tomczak, 1992). ILD broadly concurs with MLD (based on density criteria) throughout the majority of the global ocean due to the strong influence of the thermocline. Yet, there are other cases where ILD
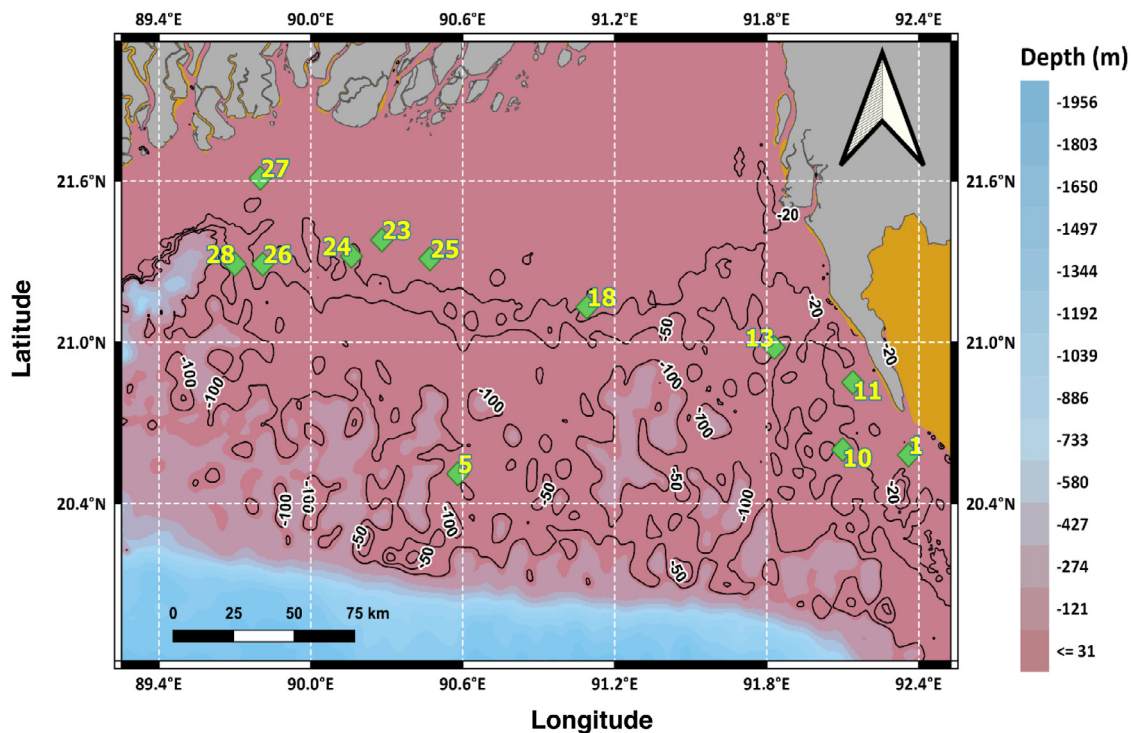
Fig. 2. Bathymetry of the northern Bay of Bengal (colors and black lines, in m), located at the northernmost tip of the Indian Ocean. Sites for in-situ profiles taken during the cruises are marked with green diamonds and labeled with yellow numbers. Light blue illustrates deeper sea while magenta depicts shallower sea. (For interpretation of the references to color in this figure legend, the reader is referred to the web version of this article.)

and MLD have noteworthy differences, controlled by the salinity distribution (Lukas and Lindstrom, 1991). If the ILD becomes deeper than the MLD, the intervening layer between the mixed layer and the top of the thermocline can be defined as a "barrier layer" (Godfrey and Lindstrom, 1989). Another opposite phenomenon known as "compensation layer" can occur in the ocean. This is an intermediate layer between the isothermal layer and the upper pycnocline, when the MLD is deeper than ILD (Rudnick and Ferrari, 1999). Usually, negative salinity stratification requires positive temperature stratification to generate a compensation layer (Weller and Plueddemann, 1996).

In addition to the 0.125 kg m^{-3} density criterion (de Boyer Montégut et al., 2004), ILD can also be defined as the depth where the temperature is 0.5 °C cooler than the SST. Strong vertical stratification, associated with high SST and low sea surface salinity (SSS), leads to the formation of a shallow mixed layer (ML) in the BoB (Vinayachandran et al., 2002). TI has a close association with the presence of thick Barrier Layer (BL), along with MLD (Chowdhury et al., 2019). BL can be obtained from the difference between the previously mentioned ILD and MLD. Both BL and ML undergo heating because of shortwave-induced radiation and net surface heat flux due to horizontal advection. However, when the heating of the BL exceeds that of the ML, a temperature inversion develops (Girishkumar et al., 2013). Moreover, as the density stratification loses its stability due to an increase in temperature with depth, salinity stratification compensates for this instability by facilitating the development of TI (Thadathil et al., 2016).

Previous studies in the BoB indicated TIs during winter (November to March) (Thadathil et al., 2002; Thompson et al., 2006; Vinayachandran et al., 2002). Specifically, the NBoB exhibits strong seasonality in TI, with TI most common in months when BL is the thickest. Surface cooling and freshwater influx in winter cause significant interannual variability in TI (Thadathil et al., 2002). This inversion peak can reach up to 1.57 °C in the BoB (Thompson et al., 2006). TI initiates in October and attains maximum intensity between 0.50 °C and 0.75 °C during this season.

In contrast, a considerably reduced TI occurs in both summer and spring; this reduced TI is related to the thinning of the BL (Thangaprakash et al., 2016). The strong solar-radiation induced warming of the surface layer, along with reduced river runoff, is a key contributor to this weakening BL in spring and summer, and thus, TI becomes trivial in these seasons. Interestingly, TI not only shows seasonal variability but also exhibits inter-annual variations (Girishkumar et al., 2013). However, the previous studies were predominantly limited to the central and southern BoB, with minimal focus on the northern portion of the BoB. Thus, more research on TI is needed to understand the ocean–atmosphere coupling process in the NBoB.

Temperature inversions are important to atmospheric and oceanic processes, particularly at the air–sea interface, as TI plays a significant role in generating SST variabilities and anomalies in the BoB (Nagura et al., 2015). A better understanding of the influence of TI on the physical processes that govern the NBoB will provide a basis for model improvement identification of forecast biases (Masud-Ul-Alam et al., 2022). Wang et al. (2012) proposed that the downward ocean heat pumping was weakened by the stratification and TI. Thus, TI impacts the intensification of tropical cyclones. TI additionally affects vertical mixing that feeds back to SST in the BoB (Mathew et al., 2018). This phenomenon makes studying TI more essential for the coastal states, as the intensity (of both surface winds and rain potential) of the cyclone at landfall largely corresponds to the initial conditions of ILD and variations in TI. Although there are studies about inversions in spring, only scarce fieldwork has been conducted to study TIs in the northern shelf of the BoB, especially before the summer monsoon onset. This lack of high-resolution measurements of in-situ temperature, salinity, and other oceanic and atmospheric processes (Mili et al., 2021) further hampers research into intra-seasonal and annual evolution of the TI layer. Therefore, very few studies exist on the spatio-temporal evolution of TIs in the NBoB (Thadathil et al., 2007, 2002; Thadathil and Gosh, 1992).

In-situ spatial and temporal data are required for understanding the physical processes in the NBoB. Our study uses in-situ physio-chemical measurements obtained during very recent cruises that occurred in January, February, and March 2020. Since in-situ data from the cruises are restricted to a 50-meter depth contour of the Bangladeshi shelf region, the focus of this study is on two parts of the least-studied area of the NBoB (Fig. 2): the eastern (91°E to 92.1°E, 20.5°N to 21.2°N) and western (89.5°E to 90.5°E, 21.1°N to 21.6°N) parts of the NBoB. The primary reason for defining these two regions in such a way is to maximize the benefits from the cruise stations locations, which are clustered in the eastern and western parts of the NBoB.

The NBoB is a data-poor region, and comprehensive in-situ measurements have been largely limited. In a previous study, Narvekar and Prasanna Kumar (2014) averaged 7197 Hydro-cast, 2714 Conductivity, Temperature, and Depth (CTD), and 4569 Argo profiles of temperature and salinity in the BoB and plotted those in 1° × 1° degree grid. That study revealed the acute deficit of data in the wide and shallow coastal area (20°N–22°N), with many of the coastal grids containing no data at all. This study provides in-situ CTD profiles taken during the winter in the data-dearth region, between 19°N and 21.6°N. It therefore fills not only the data unavailability but also the gaps left by previous studies, connecting the dots of previous studies to provide new understanding about thermal inversions in the northern BoB.

2. Materials and methods

2.1. In-situ profiles

The in-situ measurements were made during three cruises: the first on 2 January 2020, the second from 8 to 9 February 2020 onboard the Bangladesh Navy ship *Sangu*, and the third from 18 to 21 March 2020 onboard fishing vessel *Salman-2*. These measurements covered both the winter and spring monsoon. All three expeditions covered 12 stations in total, and temperature, salinity, and density profiles were taken in each station using a single-fire module using the Sea and Sun Technology (GmbH) conductivity, temperature, and depth (CTD) instrument. A total of 12 profiles were made to depths of 50 m. These CTD profiles directly measure temperature (accuracy: ± 0.002 °C), conductivity (accuracy: ± 0.002 mS/cm), and pressure (accuracy: up to 0.05% full scale within the range of –5 °C to 35 °C). Salinity was acquired from the conductivity, and density was calculated from temperature and salinity. This raw CTD data was processed into a more user-friendly netCDF format for convenient data analysis and visualization (Masud-Ul-Alam et al., 2020b,a). For ease of analysis, the stations were grouped into two zones and designated as north-western BoB (NW-BoB) and north-eastern BoB (NE-BoB). The NW-BoB contained vertical profiles (Fig. 3) from stations 5, 23, 24, 25, 26, 27, and 28, while the NE-BoB contained vertical profiles from stations (Fig. 4) 1, 10, 11, 13, and 18.

The eastern and western stations were averaged to generate two average profiles, one for the NE-BoB and one for the NW-BoB. Measurements of two stations in the western region were taken during high tide, whereas the other two stations profiles were acquired at low tide. These stations were averaged separately by their tide criteria and plotted as vertical profiles. To identify the prevailing water masses in the locations of the profiles, the CTD data were plotted on temperature–salinity distribution (T-S) diagrams following the methods of Ning et al. (2019). A summary of the physical parameters of all stations was shown in Table 1.

2.2. SST, SSS, and surface current reanalysis

Reanalysis data were used in this study to complement the locations covered by the cruises. Several other data sources were also used to understand the thermal inversion and other physic-ochemical processes ongoing in the NBoB. First, the globally gridded 0.25° daily Optimum Interpolation Sea Surface Temperature (daily OISST), from January to March 2020, was used to analyze surface temperature in both the NE-BoB and NW-BoB (Reynolds et al., 2002). This SST dataset is based on input from several platforms' measurements and observations. Over the same time period and with a similar gridded optimal interpolation, in-situ and satellite SSS data at weekly (Droghei et al., 2016; Nardelli et al., 2016) and monthly (E.U. Copernicus Marine Service Information, 2020) scales were used to analyze surface salinity in the NE-BoB and NW-BoB. This SSS dataset is based on in-situ and satellite observations and is comprised within the same period and similar grid with optimal interpolation as the SST data. The Global ARMOR3D L4 dataset was used to understand subsurface temperature variations. This dataset has 3-D temperature and salinity on a 0.25° by 0.25° lat–lon grid at 33 depth levels, and it the L4 dataset is generated using in-situ and satellite observations (Guinehut et al., 2012). Similarly, weekly mean depth-wise (0 m to 65 m) salinity and temperature data in near real-time (NRT) were extracted from the ARMOR3D L4 dataset to compensate for the inability to retrieve satellite salinity estimates below the surface. Current speed was taken from the combined Copernicus Marine Environment Monitoring Service (CMEMS) NRT satellite daily mean geostrophic surface currents and modeled Ekman currents, available in a 0.25° by 0.25° lat–lon grid from January to March 2020 (Rio and Mulet, 2014).

2.3. Calculation of mixed layer depth and thermal inversion

Vertical profiles of temperature, salinity, and density (up to the maximum depths of each station) were plotted using PyFerret (a Unix-based program developed by the NOAA Pacific Marine Environmental Laboratory). We adopted the density criterion proposed by Kara et al. (2000) to define the MLD. This method incorporates UNESCO's state equation (Eq. (1)), where the MLD is calculated with a fixed temperature difference ($\Delta T = 0.8$ °C) at a reference depth of 10 m (Kara et al., 2003):

$$\Delta d = \Delta \sigma_{t*} (T_s + \Delta T, S_s, P_s) - \Delta \sigma_t (T_s, S_s, P_s) \tag{1}$$

where the density difference is denoted by Δd from the surface to the MLD's bottom; σ_{t*} represents density equivalent to the ΔT changes of the SST (T_s) while keeping the salinity fixed; σ_t corresponds to the density at the surface (kg m^{-3}), and S_s, and P_s, are surface salinity and pressure, respectively. We estimated ILD and TI were estimated following Kumari et al. (2018). Following the threshold method, the depth at which the temperature (or density, sigma-t) exceeds the surface value at a specific temperature or density (a difference of 0.2 kg m^{-3} density in this study) can be defined as the mixed layer depth (MLD) in a vertical profile (Masud-Ul-Alam et al., 2020b,a; Narvekar and Prasanna Kumar, 2006). The depth at which the temperature decreases by 0.8 °C from the SST was considered as the ILD. Additionally, the positive difference between the ILD and MLD was chosen as the BLT.

2.4. Spatio-temporal evolution and time series of SST, SSS, and surface current

Time series plots of SST, SSS, and surface current were created by averaging the values from the NE-BoB and NW-BoB. These
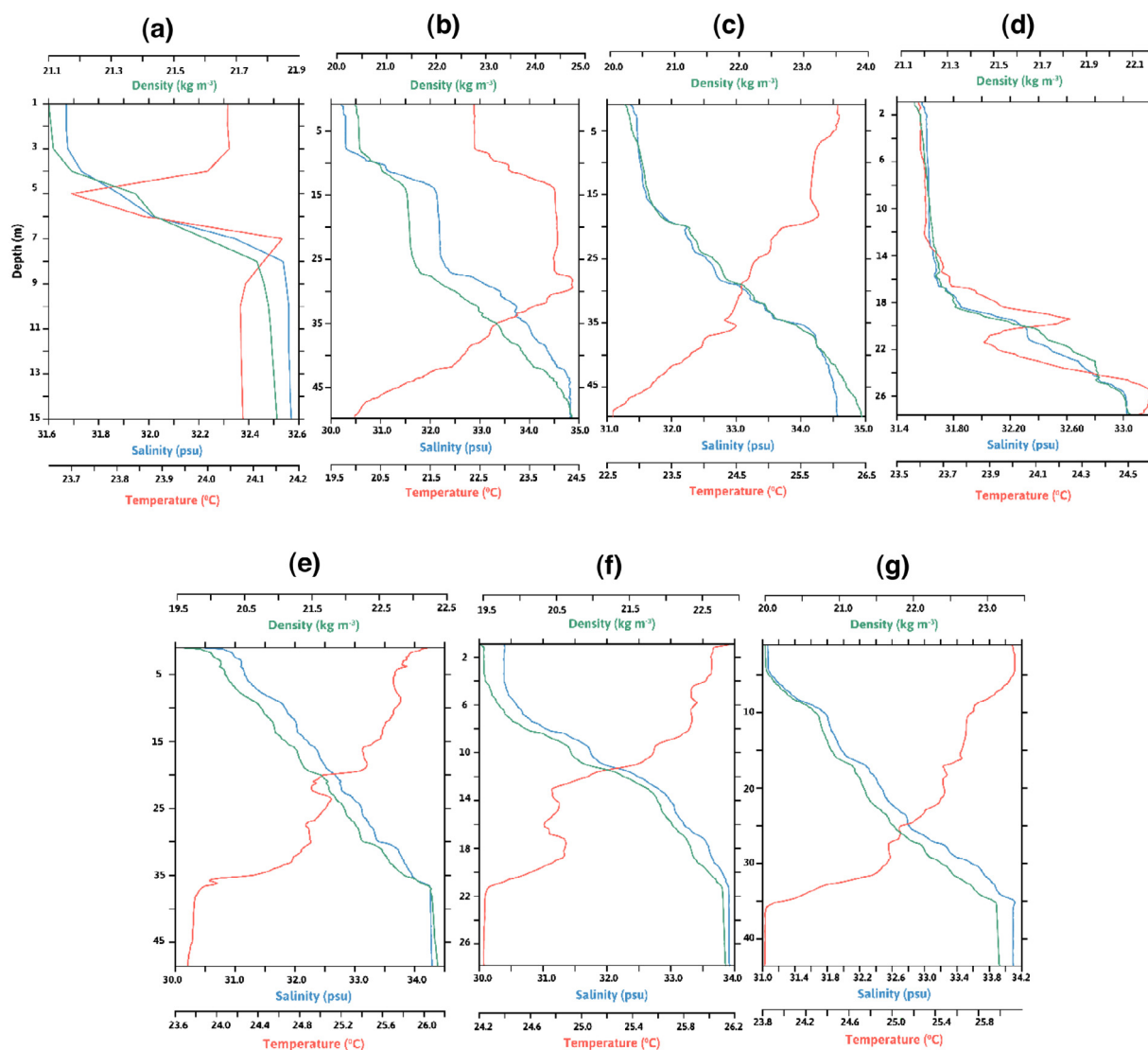
Fig. 3. Vertical CTD profiles of temperature, salinity, and density against depth of stations 5, 23, 24, 25, 26, 27, 28 (from a to g) located in the northwestern BoB (89.5°E: 90.5°E; 21.1°N to 21.6°N). Temperature is represented by orange lines, blue lines represent salinity, and light green lines represent density. (For interpretation of the references to color in this figure legend, the reader is referred to the web version of this article.)

Table 1
Summary of the temperature, salinity and density profiles and their oceanographic features.

St. No	Thermal inversion-1		Thermal inversion-2		Presence of deeper cold water (m)	Tide height (m)	Mixed layer depth (m)	Current speed (m/s)
	Range (m)	Temp Diff (°C)	Start (m)	Temp Diff (°C)				
5	16–20	0.2	34–36.5	0.28	n/a	0.99 LT-2	7.13	0.03
10	18–20	0.7	n/a	n/a	n/a	−0.07 LT-2	7.93	0.23
1	7.3–9	0.23	n/a	n/a	10–15	2.55 HT-5	4.62	0.16
11	16–20	0.45	22.5–27	0.2	38–48	2.51 HT-3 (ebb)	1.14	0.18
13	n/a	n/a	n/a	n/a	36–43	0.69 LT-5	6.46	0.24
18	13.5–16	0.05	17–19	0.2	22–27	2.76 HT-last	5.77	0.29
25	12–19.5	1.2	n/a	n/a	43–48	−0.36 LT-3	7.77	0.14
23	27–32	0.6	n/a	n/a	n/a	−0.36 LT-last (flood)	8.64	0.14
24	12.5–19.5	1.2	24–30	0.5	n/a	−0.36 LT-1	8.24	0.06
26	8–21.5	1.5	n/a	n/a	n/a	3.34 HT-5	8.39	0.21
28	16–19	0.49	n/a	n/a	n/a	3.34 HT	13.4	0.27
27	16.5–21	0.48	24.3–27	0.65	n/a	3.34 HT-2	18.58	0.43

cross-sectional plots (also known as Hovmöller diagram) were compared to the station profiles. Finally, the averaged cross section of temperature in both eastern and western sections of the NBoB was also examined.

3. Results

The main results of the study can be summarized as follows: (1) Relatively deeper ILD was detected at the NW-BoB, compared
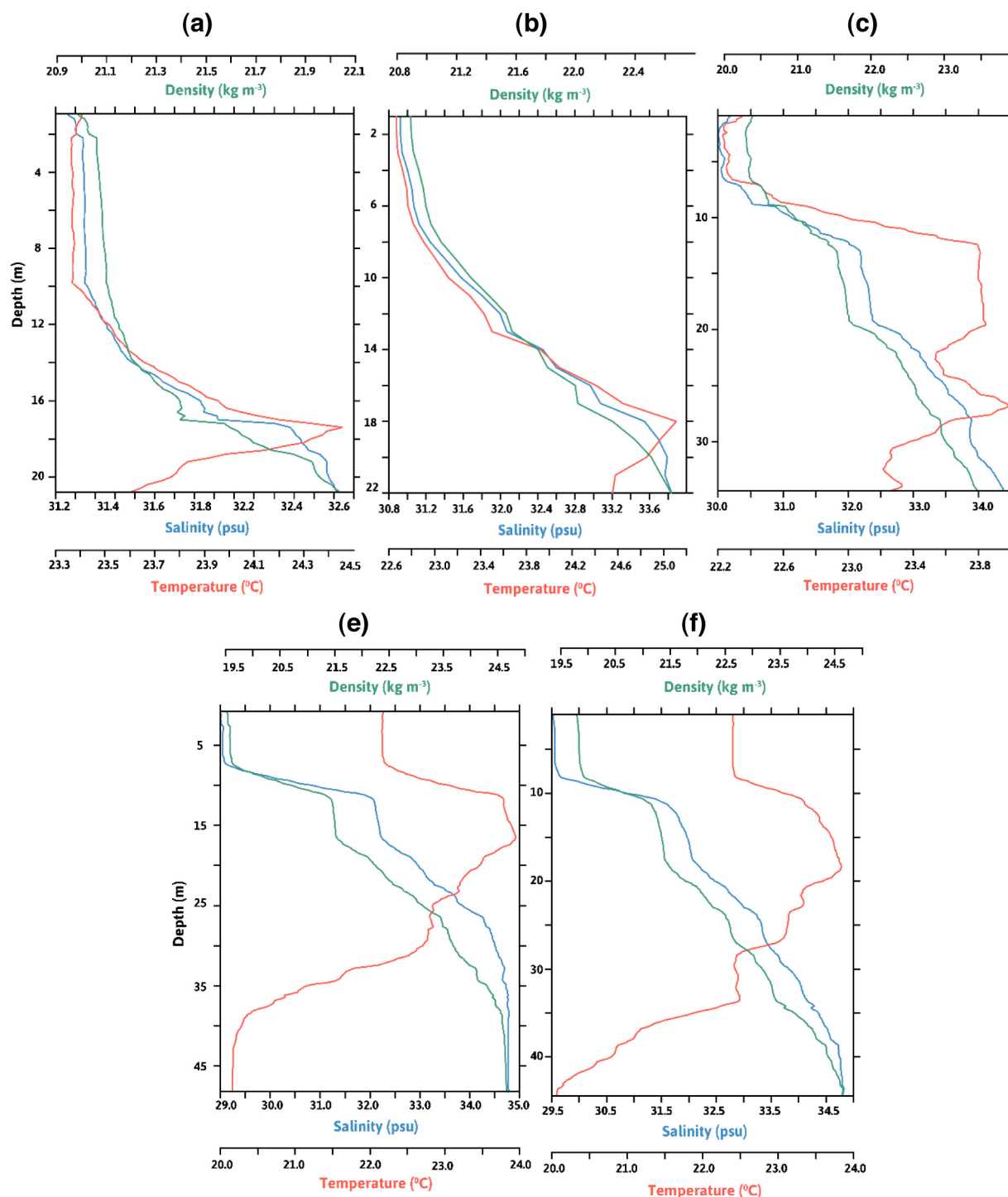
Fig. 4. Same as Fig. 4, except for stations 1, 10, 11, 13, and 18 (from a to f) located in the northeastern BoB (91°E to 92.1°E; 20.5°N to 21.2°N).
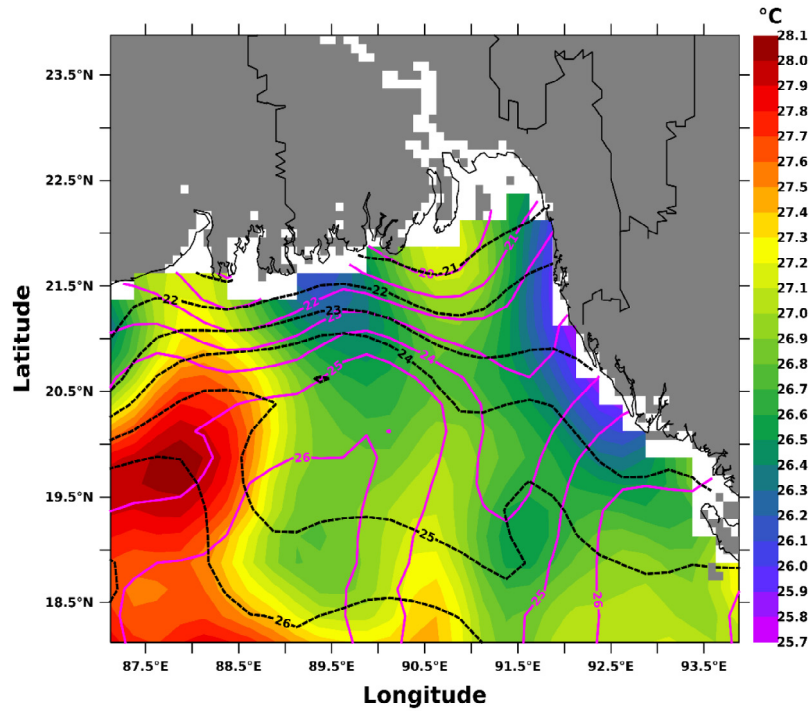
to the NE-BoB (estimated based on the vertical profiles of Temperature, Salinity and Density), (2) TI at different depths was noticed in a few of the stations (5, 11, 18, 24, 27), (3) Three different water masses (BoBLSW, BoBIW and PCW) were identified from the profiles taken during the cruise.

3.1. Vertical profiles of temperature, salinity, and density

Stations in NW-BoB generally possessed higher MLD and ILD (Table 1) compared to their eastern counterparts, with the average MLD being 10.3 m. The NW-BoB stations (Fig. 3a–g) presented

comparatively deeper ILD (8.4 m) than that of the NE-BoB (3.7 m). Two stations (26, 27) in the NW-BoB did not show any ILD (they were well-mixed near the bottom layer), but all stations in the NE-BoB showed the presence of ILD. Although the deepest ILD measured from January–March was around 12 m, it also fluctuated from as shallow as 3 m to as deep as 12 m. The BLT was identified at station 23 and 25 in the NW-BoB, with values of 1.35 m and 4.22 m respectively. In the opposite portion of the bay, stations 1, 13, and 18, in the NE-BoB (Fig. 4 a–f) had BLT of 0.38 m, 0.54 m, and 2.23 m, respectively. Thus, the NW-BoB had an overall shallower BLT than did the NE-BoB. Station 27 had
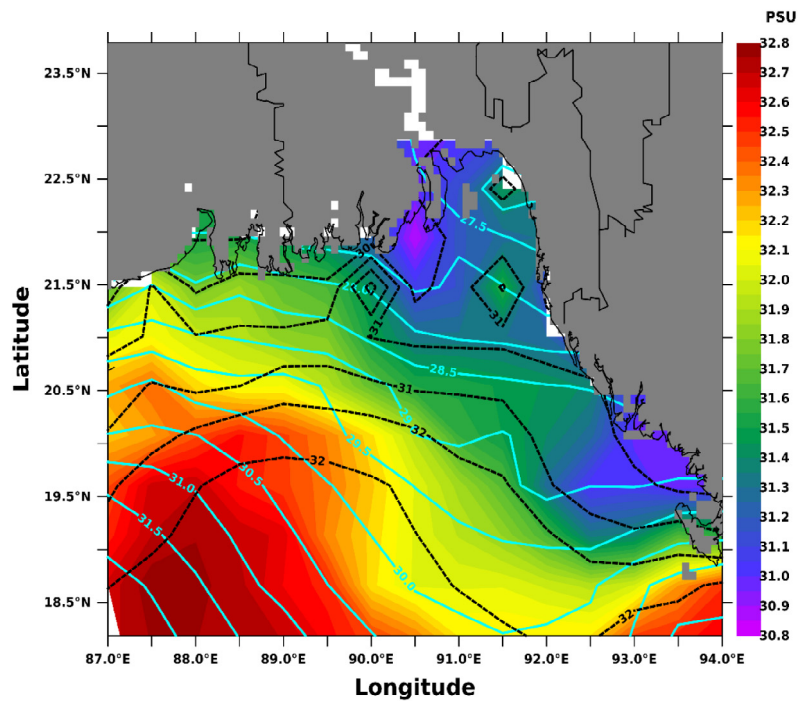
Fig. 5. Surface plots of (a) temperature and (b) salinity in the northern Bay of Bengal using globally gridded 0.25° daily Optimum Interpolation Sea Surface Temperature (daily OISST) and optimal interpolation, in-situ and monthly satellite observation Sea Surface Salinity (SSS). Purple, black contour, and color fill represent SST for January, February and March while cyan, black contour, and color fill represent SSS for January, February and March, respectively. (For interpretation of the references to color in this figure legend, the reader is referred to the web version of this article.)

the MLD farthest from the surface, at 18.58 m. In contrast, the MLD decreased by almost half when transitioning from the NW-BoB to NE-BoB. Mean MLD throughout the stations in NE-BoB was around 5.18 m, the deepest MLD in the NE-BoB was found at station 10 at 7.93 m.

3.2. Variation in surface temperature and salinity

Daily OISST data revealed that January was the coldest and March was the warmest month during the study period, as the SST varied from 21 °C in the north to 26 °C in the south (Fig. 5a).
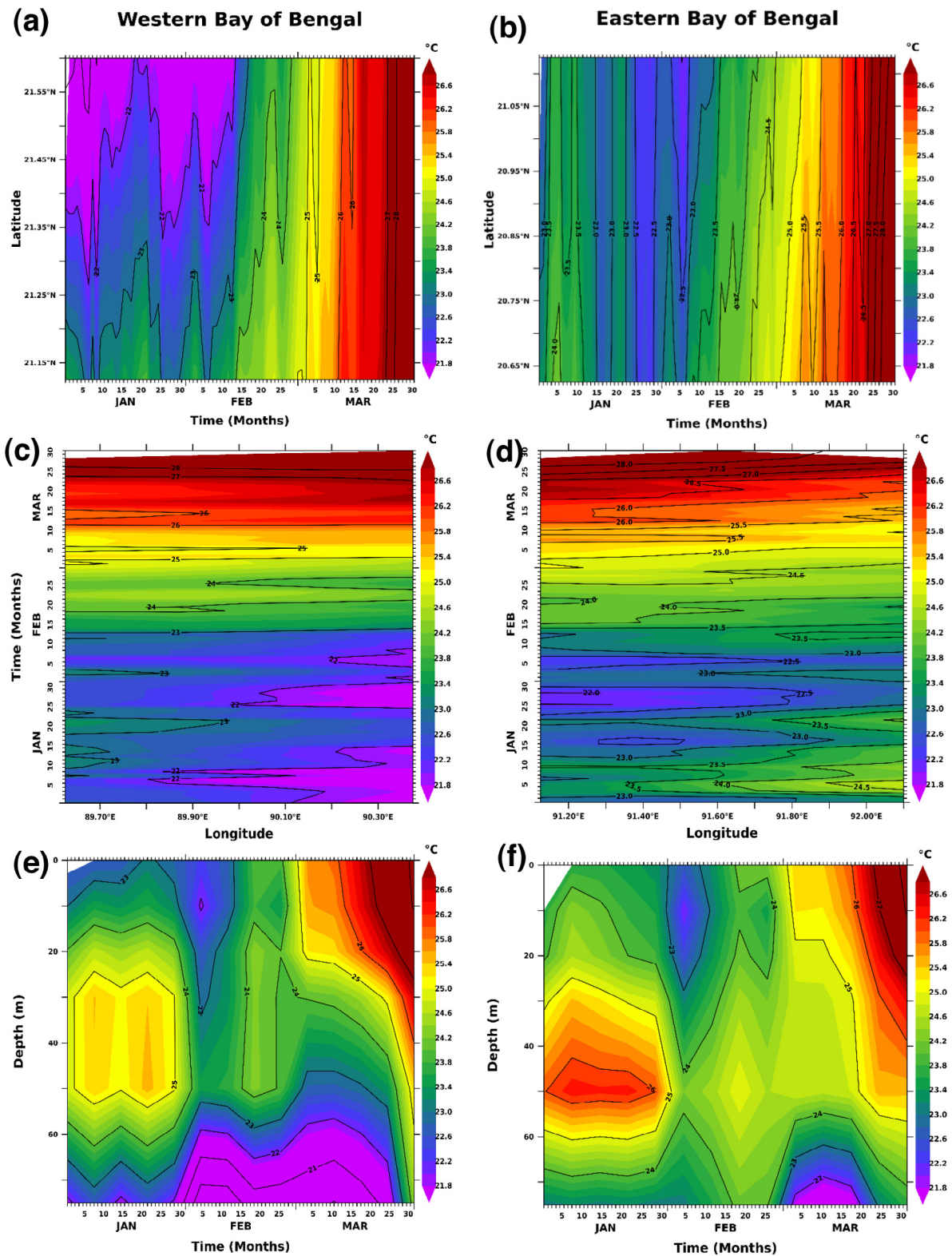
Fig. 6. Latitude vs. Time (a, b), Time vs. Longitude (c, d), and Depth vs. Time (e, f) plots of weekly mean temperature in the both eastern and western parts of the NBoB, extracted from Global ARMOR3D L4 dataset. Reddish colors characterize higher temperatures while bluish colors characterize lower temperatures. (For interpretation of the references to color in this figure legend, the reader is referred to the web version of this article.)

SST increased in the north to 26.8 °C at March, whereas the increase was not as intense in the south as it remained around 27.5 °C. In the NBoB, sea surface salinity (ARMOR3D) featured a

gradual decrease from west to east (Fig. 5b). Intrusion of high-salinity water (32 PSU) from the southwest was most prominent in February. However, the freshwater started to become

Table 2
Water masses in the Bay of Bengal, identified from current and the previous studies.

Water mass	Location	Depth (m)	Potential temperature (°C)	Salinity (PSU)	Density (kg m^{-3})	References
Bay of Bengal Low Salinity Water (yellow)	20.4°N–20.6°N, 90.6°E–90.8°E,	11	23.5–24	31.8–32.6	1021.3–1022	Present Study
Preparis Channel Water Mass (green)	21°N–21.2°N, 91.8°E–92°E	35	22.4–23.5	33.2–34.3	1022.6–1023.5	
Bay of Bengal Intermediate Water (blue)	21.4°N–21.6°N, 89.6°E–89.8°E	40	24.6–24.9	33–33.8	1022–1022.9	
G–B dominated Bay of Bengal Low Salinity Water	18.76°N, 87.00°E	5	27.521	32.020	1020.31	Singh et al. (2012)
Bay of Bengal Subsurface Water	16.76°N, 86.99°E	70	23.162	34.747	1023.69	
Arabian Sea High Salinity Water	14.42°N, 69.42°E	65	26.347	36.514	1024.07	
North Indian Intermediate Water	14.42°N, 69.42°E	500	11.677	35.506	1027.04	
North Indian Deep Water	14.42°N, 69.42°E	2100	2.717	34.814	1027.76	
Indonesian Throughflow Intermediate Water	9.99°S, 101.98°E	5	29.738	33.912	1021.002	Amakawa et al. (2000)
Indonesian Throughflow Intermediate Water	11.50°S, 115.95°E	1099	4.470	34.612	1027.43	Jeandel et al. (1998)
Modified North Atlantic Deep Water	27.01°S, 56.97°E	3100	1.774	34.739	1027.78	Bertram and Elderfield (1998)
Antarctic Bottom Water	59.58°S, 60.98°E	4709	−0.615	34.665	1027.87	Kumar and Li (1996)

dominant over at the NBoB especially near the northern and northeastern coast.

3.3. Spatio-temporal variability in temperature and salinity

A gradual increase in temperature with time was visible in latitude (Fig. 6a–b) and longitude (Fig. 6 c–d) plots of the western and eastern NBoB. January is characterized by relatively colder temperatures (22 °C), especially in the northern (21.4°N–21.6°N) and eastern (90.1°E–90.35°E) parts of the NW-BoB. Temperatures in these subregions gradually increased in February and March, stabilizing around 25 °C and 28 °C, respectively. Interestingly, the western parts of the NBoB were warmer than their eastern counterparts, with a maximum difference of around 2.5 °C in January. Periodic rises and falls in temperature were noticed across all latitudes; however, it was generally warmer in the east as the temperature progressively peaked in February and March. A warm layer of 25 °C–26 °C, between 26 m and 53 m depth in the west (Fig. 6e) and 26 m and 58 m in the east (Fig. 6f), was located between colder water (24 °C) at surface and bottom during January. This warm layer cooled down (∼2 °C) in February and March. But, the magnitude of this cooling varied east to west, and the NE-BoB was warmer whereas the deeper portion of the NW-BoB was cooler. Presence of such warm water parcel in January is also evient from the climatological (1993–2020) section plots in the NE-BoB and NW-BoB (Fig. S1a-S2a). Temperature in the study region varied both by latitude and longitude in January, especially in the western block. We noticed

a layer of warm water (25 °C) at 20 m depth in the NW-BoB (Fig. 7a), similar to the fusion of warm water (24.5 °C) at other longitudes (Fig. 7b). The general pattern suggested that temperature decreased with depth. An exception to this pattern was in the NE-BoB (Fig. 7c), as warmer water (25.2 °C) existed between two comparatively colder layers (24.5 °C), especially between 40 m and 50 m. Likewise, warmer layer at similar depths persisted from 91°E to 92.1°E (Fig. 7d). Lower saline water of 29 PSU in the north confronts higher saline water of 29.4 PSU in the south (Fig. 8 a–b). On the contrary, in the meridional averaged (Hovmöller) plots revealed further variations (Fig. 8 c–d) of low (high) saline water in January to mid-February (mid-February to March). Hovmöller plots (depth vs. time) for the western region (Fig. 8e) depicted less salty water at the surface and gradually increased with depth, from January to February. However, we observed an intrusion of high salinity water (34.5 PSU) from 40 m to 60 m depth in March. Contrastingly, the NE-BoB was (Fig. 8f) relatively fresh water (<30 PSU) in January. While salinity gradually increased with depth in February, comparatively high salinity water (34.5 PSU) existed at 60 m in both January and March. Climatological data (Fig. S1b-S2b) of salinity also depicted fresher (29.5 PSU) surface water in the NE-BoB's surface and high salinity in each region's 60 m depth.

3.4. Zonal averaged profiles

The stations in the NW-BoB (Fig. 9a) indicated stable physical conditions down to 8 m depth. TI in this region was not as intense
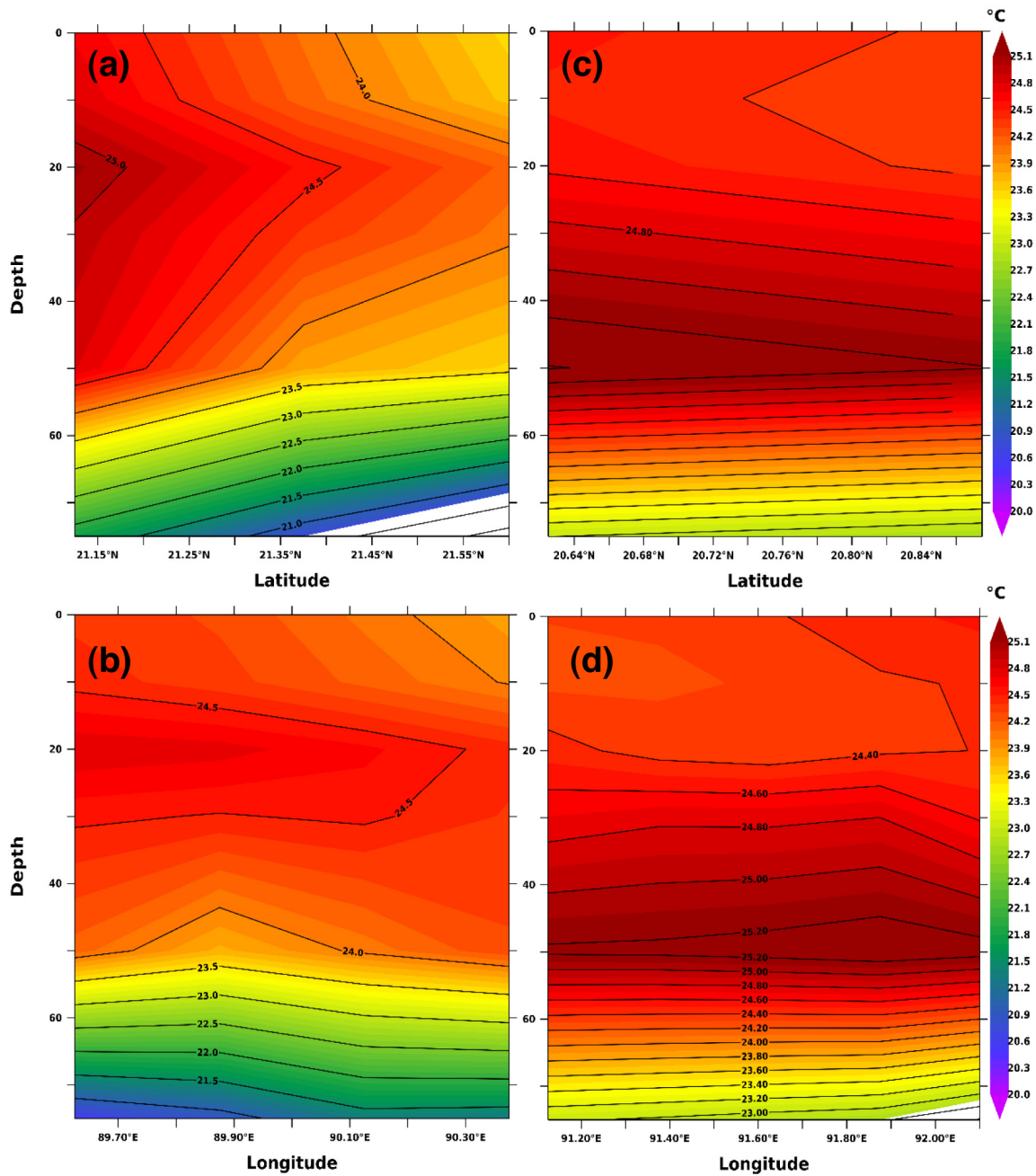
Fig. 7. Averaged section plot of temperature in both the NW-BoB (a, b) and NE-BoB (c, d), extracted from Global ARMOR3D L4 dataset Reddish colors characterize higher temperatures while bluish colors characterize lower temperatures. (For interpretation of the references to color in this figure legend, the reader is referred to the web version of this article.)

as the previous one (NE-BoB). An average inversion temperature by 0.58 °C is observed at 9 m depth. Averaged profiles of NE-BoB stations (Fig. 9b) demonstrated two TI layers, one located at 5 m and another at 28 m depth. The inversion strength was 0.6 °C and 0.37 °C, respectively.

3.5. Averaged high and low tide profiles

Averaged high tide stations in the NW-BoB revealed stable temperature, salinity, and density until 14 m depth (Fig. 10a). The MLD was located at 14 m, and a TI of 0.28 °C is found between 16.5 m to 20.5 m. On the contrary, the low tide stations (Fig. 10b) in the NW-BoB featured two TI layers. The first one was located from 9 m to 17 m depth, with a temperature difference of 1.5 °C,

and the second one was located from 26 m to 28 m depth, with a (smaller) temperature difference of 0.1 °C.

3.6. Pattern in thermal inversion

Some of the stations (5, 11, 18, 24, 27) featured TIs at multiple depths (hereafter referred to as deeper thermal inversion, DTI). In the NBoB, there was not a meaningful east–west pattern in TI. TI in the NW-BoB ranged between 8 m and 32 m, but TI in the NE-BoB ranged between 7.3 m to 20 m. The largest TI was 1.5 °C at station 26 in the NW-BoB, and the smallest TI was 0.05 °C at station 18 in NW-BoB. DTI in the NW-BoB were mostly located at greater depths, ranging from 24 m to 36.5 m, with a mean change
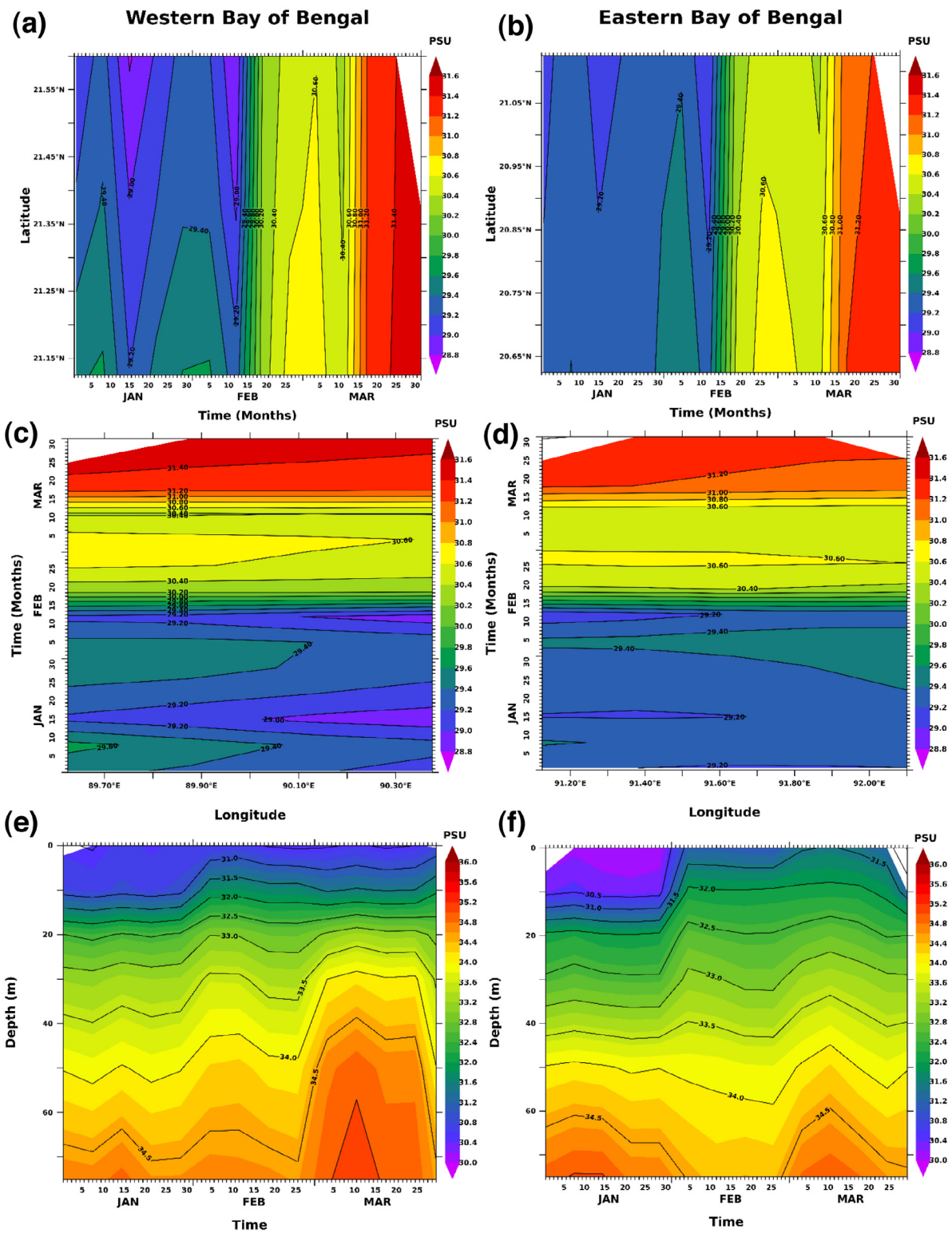
Fig. 8. As in Fig. 6 except that the reddish colors characterize higher saline zones while bluish colors characterize lower salinity zones.

of 0.5 °C. However, the DTI in the NE-BoB was shallower, between 17 m and 27 m, with a mean change of 0.2 °C. The eastern bay was generally cooler, hence the MLD attained shallower depth. A relatively colder layer of 24.4 °C to 24.6 °C stays on top of warmer waters in the section (depth-latitude) plot. The NE-BoB revealed a warmer layer (25 °C to 25.2 °C) wedged between two colder

(24.6 °C) blocks of water. While the NE-BoB featured temperature variations with depth, temperatures in the NW-BoB were mostly uniform. The western zone included warmer water at the surface with gradually declining cold water at the bottom. Colder water was located in the NE-BoB and warmer water was located in the NW-BoB.
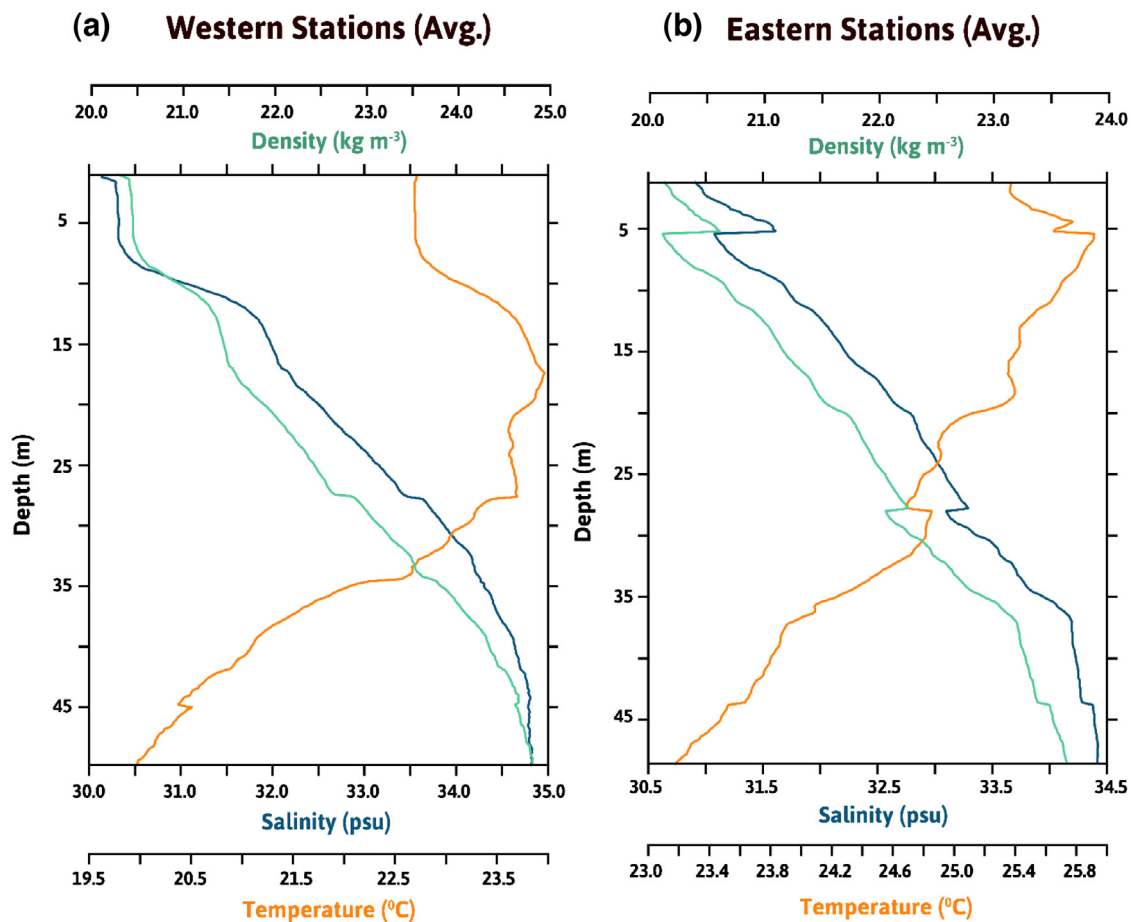
Fig. 9. Averaged temperature (°C), salinity (PSU), and density (kg m^{-3}) in-situ CTD profiles of (a) NW-BoB and (b) NE-BoB parts of the northern Bay of Bengal. Orange, Navy-Blue and Green curves represent temperature, salinity, and density respectively. (For interpretation of the references to color in this figure legend, the reader is referred to the web version of this article.)

3.7. Temporal evolution of the temperature, salinity and current speed

Temperature trends in the NW-BoB and NE-BoB were similar (Fig. 11a) in February and March; water temperatures in both regions gradually increased with the coming spring monsoon. Temporal evolution of salinity (Fig. 11b) incorporated several peaks and troughs. An abrupt rise in salinity (1.4 PSU) took place during transitioning from February to March. Both eastern and western portions were almost identical in salinity trend. The current speed (Fig. 11c) showed considerable variability in the eastern and western NBoB, although the current speed were similar in January. Currents speed were higher (~0.1 m s^{-1}) in February and March, in the NE-BoB than the NW-BoB. Therefore, currents are much stronger in the east with speed up to 0.32 m s^{-1}.

3.8. Characteristics of the water masses

Three potential water masses were identified from the T–S diagram (Fig. 12). Two were found in the NE-BoB (referred to as Bay of Bengal Low Salinity Water Mass and Preparis Channel Water Mass) and a third was found in the NW-BoB (denoted hereafter as the Bay fo Bengal Intermediate Water). Bay of Bengal Low Salinity Water Mass (BoBLSW) had a density of between 1021.3 kg m^{-3} and 1022 kg m^{-3}. It was a moderately warm (23.5 °C to 24 °C) and low saline (31.8 PSU to 32.6 PSU) water. The other water mass, Preparis Channel water mass (PCWM), featured low temperature (22.4 °C to 23.5 °C) and higher salinity (33.2 PSU to 34.3 PSU) and density from 1022.6 kg m^{-3} to 1023.5 kg m^{-3} isopycnal, which makes it the densest of the three. Finally, the Bay of Bengal Intermediate Water (BoBIW) was the warmest (24.6 °C to 24.9 °C), with moderate ranges of salinity (33 PSU to 33.8 PSU) and density (1022 kg m^{-3} to 1022.9 kg m^{-3}). Section plots in the NE-BoB showed that cooler water (24.3 °C to 24.6 °C) intruded from 21.1°N, towards 20.9°N at around 5 m to 20 m depth. This temperature range coincides with the BoBLSW since it the warmest water mass among the three sampled in this study. However, it is colder than the deeper water (deeper than 50 m). The presence of warm temperature (characterized as BoBIW) extended from the north to the south of the NBoB and showed its signature in the stations of the NE-BoB as well. The fluccutuation in the temperature, salinity, and density occured as the colder water from river discharge overlayed warmer (25.3 °C to 25.4 °C) mixture of Arabian seawater and BoBIW at 60-m depth, which was located between 20.64°N and 20.85°N. In addition to the eastward transport of the BoBIW, the NE-BoB was feed by another intrusion of water that had properties separate from its upper and bottom layers. Warm (25 °C to 25.2 °C) seawater was evident throughout the longitude of NE-BoB. The characteristics of the speculated water masses are summarized in Table 2.

4. Discussion

The temporal evolution of salinity was very similar for both the NW-BoB and NE-BoB. In both regions, there was a swift drop
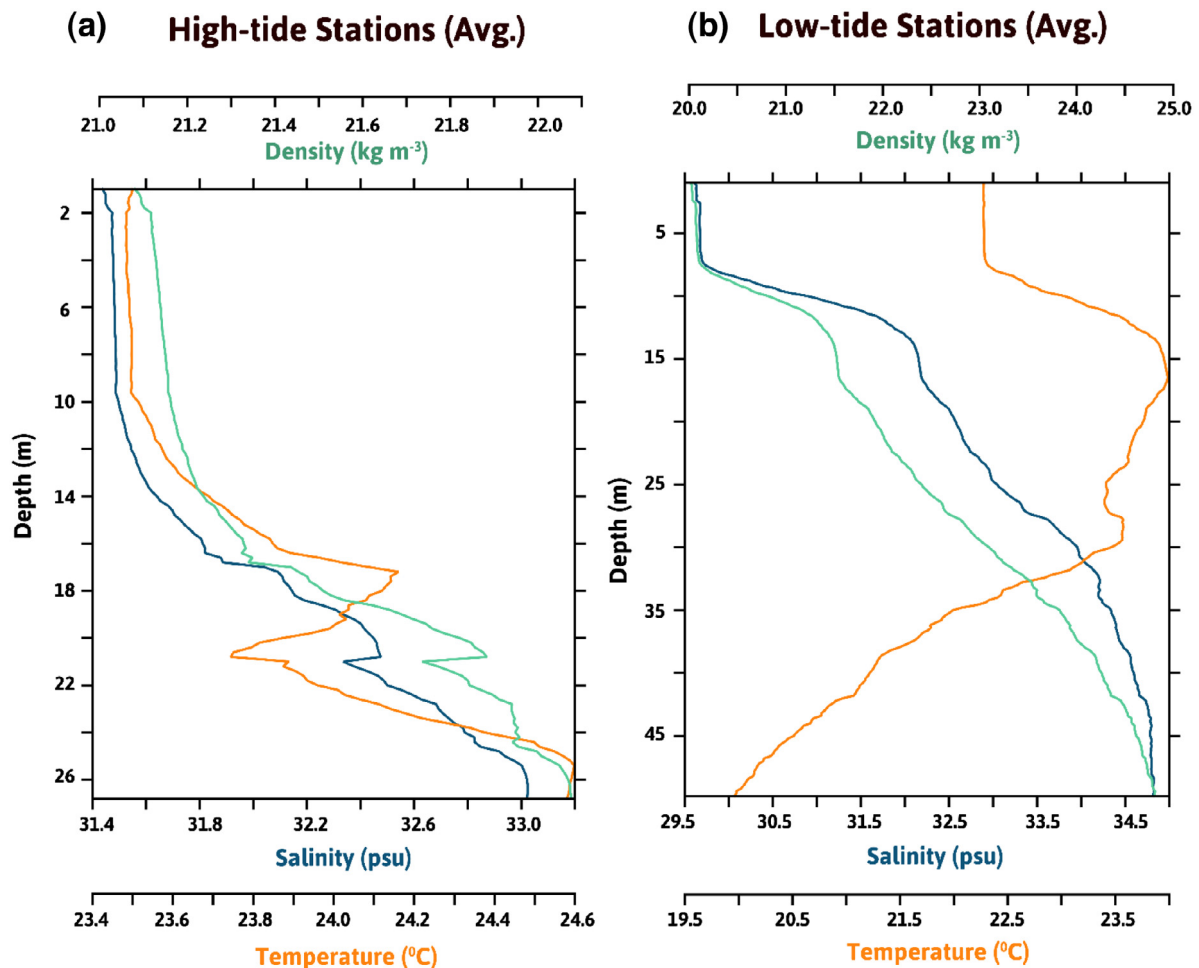
Fig. 10. Temperature (°C), salinity (PSU), and density (kg m^{-3}) in-situ CTD profiles of two high tide stations (7 & 8) and two low tide stations (11 & 12).

in salinity in the middle of each three months. In the NW-BoB, the MLD is deeper and vertical mixing is stronger, in association with the surface wind speed of the NW-BoB. Lesser vertical mixing and a shallower MLD are induced by the presence of weak wind. Stations in the NW-BoB are located nearby a major river system. Along with a massive river influx, this region receives immense rainfall that eventually ensues stratification in the water column because of the reduced salinity. Comparatively colder and fresher waters are distinct throughout the eastern region of the study area (Fig. 5), especially between 90°E to 90.4°E. This is also true for the subsurface waters (Fig. 8e–f), where the salinity of NW-BoB did not surpass 27 PSU, whereas its eastern counterpart had salinity as high as 34 PSU. This less saline, more stratified water was associatd with a deeper MLD in the NW-BoB.

Variations in MLD were well correlated to both atmospheric forcing (Alexander and Penland, 1996) and regional oceanographic characteristics (Trott et al., 2019). Although solar radiation remains a key factor in stronger stratification and lesser MLD, we did not consider that because all CTD profiles were in the period of winter to early spring (variation in intraseasonal solar radiation is small in this short period). Stations in the NE-BoB are characterized by warmer temperatures and greater salinity. Being comparatively farther from major rivers (the Ganges–Brahmaputra (G-B), the Pasur, and the Baleshwar in the northern BoB) than the NW-BoB, the NE-BoB is less prone to influence from the massive river water input. Therefore, advection of fresh river-water might not be sufficient to explain the shallow MLD in the NE-BoB. Wind stress could be dominant in affecting the

variations in MLD in this region. Wind effects have been previously suggested by Gopalakrishna et al. (1988) as a reason for the alterations of the MLD in the northern Indian Ocean. A relatively intense southward wind is observed in January and February in the NE-BoB. Additionally, wind stress was intense at the same locations. Wind stress also impacts the MLD, especially in the upper 40 m (Narvekar and Prasanna Kumar, 2014). The combined effects of the wind stress and fresh water, shallowed the MLD in the NE-BoB. Furthermore, this part of the bay is known to exhibit seasonal upwelling. McCreary et al. (1996) demonstrated the presence of upwelling in the NE-BoB in winter.

Pang et al. (2019) proposed that the peak ILD at the northernmost zone of the NBoB is caused by strong downwelling driven by negative wind stress. In contrast with the findings of previous works, where ILD reached a maximum value of up to 85 m in winter (Kumari et al., 2018), the current study's winter profiles featured shallow ILD. The BL is generally linked with ILD, where a thinner BL would lead to a thinner ILD (Girishkumar et al., 2013). The presence of very thick BL is common in the BoB (De Boyer Montégut et al., 2007). In fact, the BL thickens further northward because the surface layer and the top of the thermocline in the NBoB possess a strong salinity gradient between them (Maes and O'Kane, 2014). Circulation patterns at the surface and freshening of the upper layer of water columns caused by precipitation and river influx are the two predominant drivers of the BLT in the NBoB (Kumari et al., 2018). In this study, the BLT attained its maximum value in February (at station 25). This time of peak BLT agrees with the results of Thadathil et al. (2008).
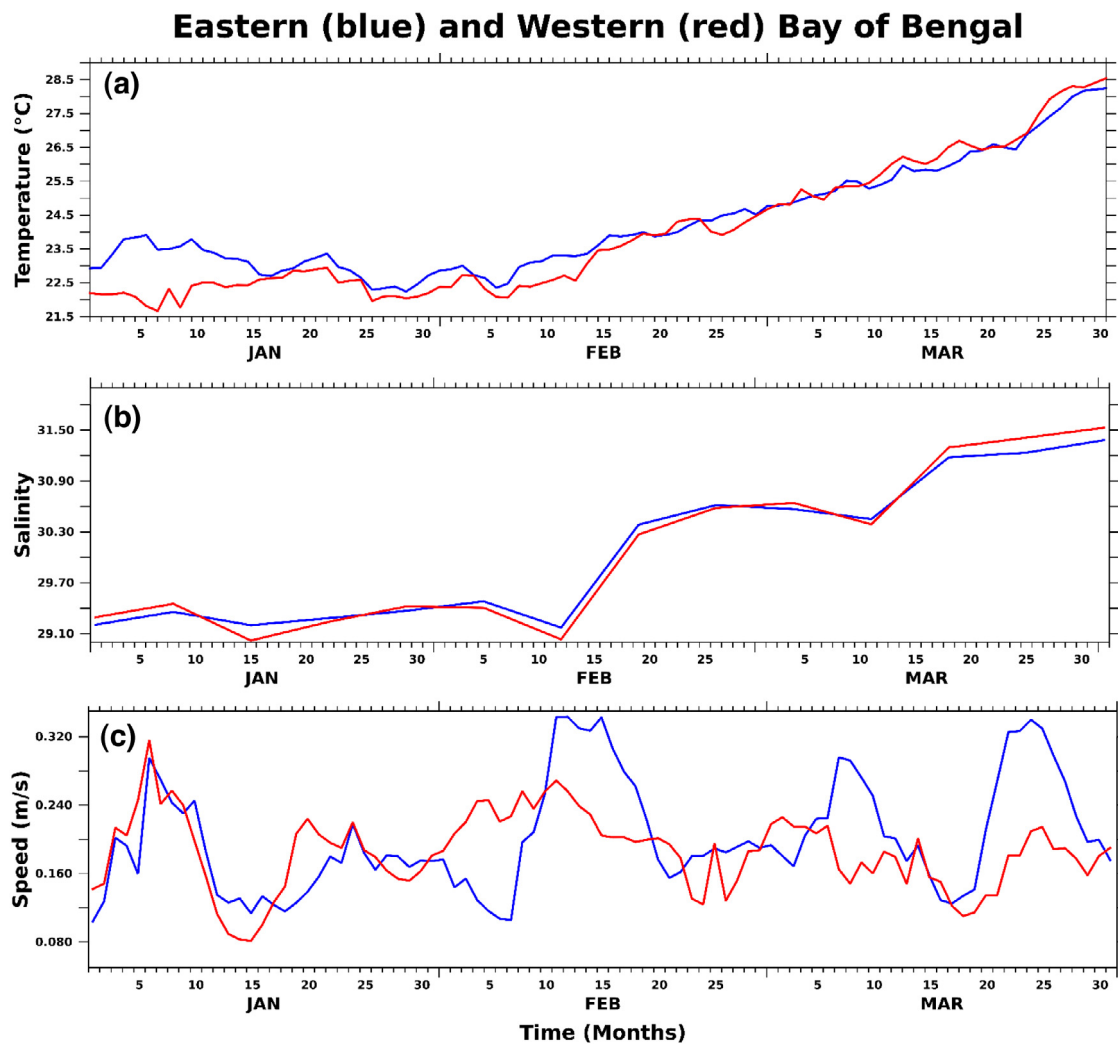
Eastern (blue) and Western (red) Bay of Bengal

Fig. 11. Average NE-BoB (blue) and NW-BoB (red) for SST (a), SSS (b) and current speed (c), from the combined product of CMEMS NRT satellite daily mean geostrophic surface currents and modeled Ekman current upon a 0.25 degree regular grid. . (For interpretation of the references to color in this figure legend, the reader is referred to the web version of this article.)

TI is very common in the BoB and exhibits strong seasonality (Shankar et al., 2002; Thompson et al., 2006). In this study, mean TI in the NW-BoB agree with Thadathil et al. (2016), who found average inversion temperatures of 0.7 °C in the NBoB. Since cooling of mixed layer can be caused by surface heat loss, TI in the NW-BoB could be induced by decrease or increase of shortwave radiation and deeper penetration of the radiation into the water column, as well as by the horizontal advection process (Girishkumar et al., 2013). The temperature inversions found at the stations in the NW-BoB are due to the heat associated with the advection of cool freshwater from the rivers, over top of the warm and saline water transported from the equatorial Indian Ocean. Temperature inversions at the stations in the NE-BoB would be caused by advection of cooler and fresher water from both the GBM river system and the Irrawady River (Thadathil et al., 2002).

Three water masses were identified in the current study. The authors hypothesize that these water masses were perhaps regulated by the two upper-ocean freshwater pathways from the BoB. The eastern pathway is situated along the western boundary of Sumatra, which often reaches as far south as the plume of ITF. The western route is placed near the east coast of India, which connects into the westward Northeast Monsoon Current (NMC) during the winter monsoon. The Indian Monsoon Current (July–September) advects warm, high salinity water mass at shallower

depths (40–100 m) from the Arabian Sea into the southwestern (SW) and central Bay during SW Monsoon. Therefore, it can be speculated that the water mass identified as BoBIW might be an extention of the Arabian Sea High Salinity Water Mass (ASHSWM) because the reversed East India Coastal Current (EICC) moved northward during February along the east coast of India carrying the ASHSWM toward NBoB. This branch further mixes with existing low salinity water near the shelf and forms BoBIW. This study suggests that warm water (24.8 to 25.2 °C) advects over cold water (23.4 to 23.8 °C) at 20 m depth in the region from 21.1 to 21.25°N.

Both Bay of Bengal Low Salinity Water Mass (BoBLSW) and Preparis Channel Water Mass (PCWM) have a more complex generation mechanism. Some of the NE-BoB profiles were taken in March where currents start to weaken and change directions since it is the end of the winter monsoon. These stations also were impacted by an annual current cycle along the eastern boundary, as mentioned by McCreary et al. (1993). Though the density of BoBLSWM (1021.5 to 1023.0 kg m^{-3}) agrees well with G–B Dominated Bay of Bengal Water Mass (Singh et al., 2012), the temperature varies by 4 °C. Therefore, we cannot confirm the association of these two watermass. This low salinity water referred in the study as Bay of Bengal Low Salinity Water Mass (BBLSW), largely occurs because of the influence of fresh water
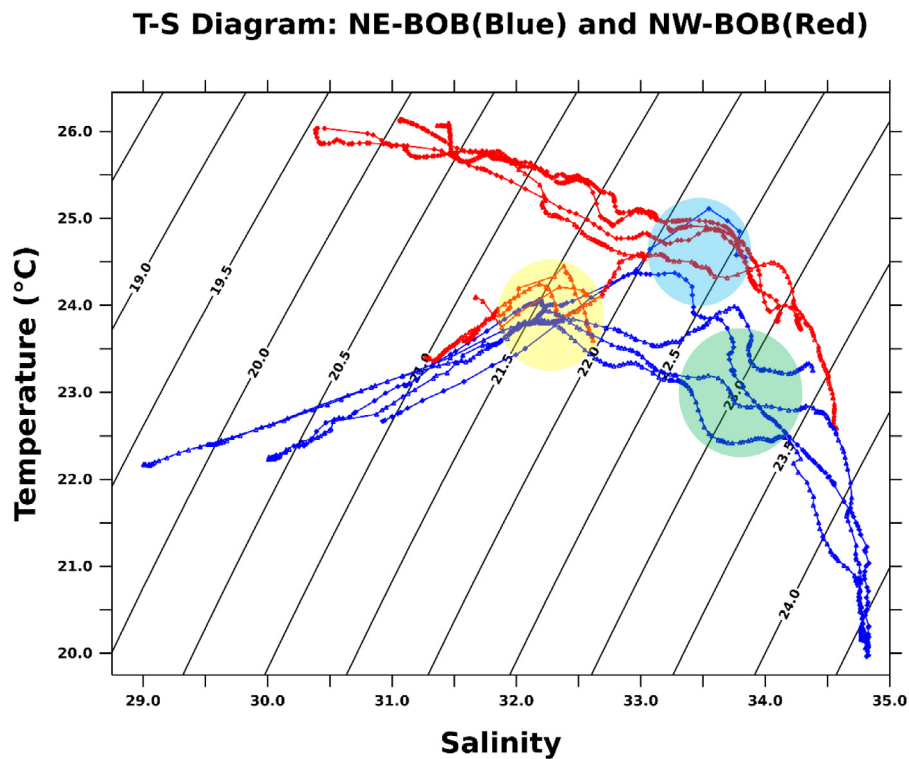
T-S Diagram: NE-BOB(Blue) and NW-BOB(Red)

Fig. 12. T-S diagram, containing profiles from all stations. Stations in the NE-BoB are illustrated by blue lines, and stations in the NW-BoB are illustrated by red lines. Three identified water masses in the figure are Bay of Bengal Low Salinity Water (yellow shaded circle), Preparis Channel Water Mass (green shaded circle) and Bay of Bengal Intermediate Water (blue shaded circle). (For interpretation of the references to color in this figure legend, the reader is referred to the web version of this article.)

brought in by several rivers near the NBoB as well as the seasonal precipitation.

Interchange between the BoB and the Arabian Sea, and subsequent feedback to water mass type in the NW-BoB, is well established (Prasanna Kumar, 2004), but there are no concrete defined water masses in the NE-BoB, especially near the northern shelf part of the NE-BoB. This could be either because there are no water masses here or this region lacks studies that focus on identifying the water masses, such as BoBLSW and PCWM. However, while investigating the northeast monsoon current in the BoB, Hacker et al. (1998) mentioned the existence of a separate water mass at the edge of the shelf break, apart from the NE-BoB region. They insisted that this water mass was influenced by Preparis eddy (14.9°N, 91.5°E), which is located the South Preparis Channel (SPC), near Andaman Sea. The water mass exchange between the Andaman Sea and the Bay of Bengal goes through three major channels, among which SPC facilitates influx of 1.36×10^6 m^3 s^{-1} in January (Liao et al., 2020). However, Raju et al. (1981) described this regions as a well mixed layer down to 100 m, with Persian Gulf water being present between 200 m to 500 m. Neverthelsss, water mass study in the junction of Andaman sea and BoB is rare. We assume that a westward flowing high saline water from the Andaman Sea through SPC and local saline water transported via north equatorial countercurrent interacts with the previously mentioned phenomena (Hacker et al., 1998). This "undefined" water mass has likely moved northward with other coastal currents and shallowed after reaching the shelf in the NE-BoB. Advected water from the rivers in the NBoB possible meets this water mass, which we define as Preparis Channel Water Mass. However, to date the water masses we found are required further detailed study with more focus on the formation and origin of the BoBLSWM, BoBIW and PCWM.

5. Conclusion

This study demonstrates spatial variability of TI during winter using in-situ CTD measurements made in the NBoB between January and March. The results revealed that the NE-BoB showed two distinct TI layers, one at 5 m and one at 28 m, with a temperature change of 0.6 °C and 0.37 °C respectively. These layers support the presence of two distinct water masses (BoBLSW and PCWM) in the NE-BoB. On the other hand, NW-BoB possessed only one TI at 8 m (0.58 °C), supporting the presence of another distinct water mass (BoBIW). In general, stations in the NW-BoB had higher MLD and ILD because of low salinity stratification, and stations in the NE-BoB had lower MLD and ILD due to seasonal upwelling. In the case of averaged high tide stations in the NW-BoB, stable temperature, salinity, and density were observed to 14 m depth with the presence of MLD. In contrast, the average stations of low tide in the NW-BoB showed two TI layers at 9 m and 17 m depth, with a change in temperature of 1.5 °C. During winter, TI peaked in the NE-BoB because of the combined contributions from the EICC and discharge of colder and less saline water from nearby rivers. This study is the first attempt to address the spatial variation of TI and watermasses in the shallow NBoB. The results here are among the first contributions to baseline information that can be useful for further studies of the thermodynamics and physical processes of the NBoB. Such a rigorous studies remain necessary to establish and validate the prevailing water masses in the NBoB. Observations over a longer period are needed to further investigate the inter-annual variability of TI in the NBoB.

CRediT authorship contribution statement

Md Masud-Ul-Alam: Conceptualization, Methodology, Software, Data Analysis, Initial Draft and Writing. **Md. Ashif Imam**

Khan: Data curation, Draft Preparation, Visualization. **Bradford S. Barrett:** Writing, Editing, Reviewing, Validating the Concepts. **Sara Rivero-Calle:** Supervising, Writing, Editing. **Md Rony Golder:** Reorganising, Editing, Writing. **Muhammad Abdur Rouf:** Reviewing, Editing.

Declaration of competing interest

Acknowledgment

Appendix A. Supplementary data

Supplementary material related to this article can be found online at https://doi.org/10.1016/j.rsma.2022.102417.

References

Alexander, M.A., Penland, C., 1996. Variability in a mixed layer ocean model driven by stochastic atmospheric forcing. J. Clim. 9, 2424–2442.

Amakawa, H., Alibo, D.S., Nozaki, Y., 2000. Nd isotopic composition and REE pattern in the surface waters of the eastern Indian Ocean and its adjacent seas. Geochimica et Cosmochimica Acta 64 (10), 1715–1727. http://dx.doi.org/10.1016/S0016-7037(00)00333-1.

Bertram, C.J., Elderfield, H., 1998. The geochemical balance of the rare earth elements and neodymium isotopes in the oceans. Geochimica et Cosmochimica Acta 57 (9), 1957–1986. http://dx.doi.org/10.1016/0016-7037(93)90087-D.

Chen, X., Sun, Z., Lin, H., Zhu, J., Hu, J., 2019. Analysis of temperature inversion in the Zhujiang River Estuary in july 2015. Acta Oceanol. Sin. 38, 167–174. http://dx.doi.org/10.1007/s13131-019-1420-8.

Chowdhury, Azam, Jiang, Wensheng, Liu, Guimei, Ahmed, Chowdhury, Sirajuddin, Chowdhury, K.M., 2019. Formation and Types of Thermal Inversion in the Bay of Bengal. CLIVAR Exch.

Clowes, A.J., Deacon, G.E.R., 1935. The deep-water circulation of the Indian ocean. Nature 136, 936–938. http://dx.doi.org/10.1038/136936A0.

de Boyer Montégut, C., Madec, G., Fischer, A.S., Lazar, A., Iudicone, D., 2004. Mixed layer depth over the global ocean: An examination of profile data and a profile-based climatology. J. Geophys. Res. Ocean 109, 1–20. http://dx.doi.org/10.1029/2004JC002378.

De Boyer Montégut, C., Vialard, J., Shenoi, S.S.C., Shankar, D., Durand, F., Ethé, C., Madec, G., 2007. Simulated seasonal and interannual variability of the mixed layer heat budger in the northern Indian ocean. In: Journal of Climate. American Meteorological Society, pp. 3249–3268. http://dx.doi.org/10.1175/JCLI4148.1.

Droghei, R., Buongiorno Nardelli, B., Santoleri, R., 2016. Combining in situ and satellite observations to retrieve salinity and density at the ocean surface. J. Atmos. Ocean Technol. 33, 1211–1223. http://dx.doi.org/10.1175/JTECH-D-15-0194.1.

Durand, F., 2004. Impact of temperature inversions on SST evolution in the south-eastern Arabian sea during the pre-summer monsoon season. Geophys. Res. Lett. 31, L01305. http://dx.doi.org/10.1029/2003GL018906.

E.U. Copernicus Marine Service Information, 2020. IN-SITU_GLO_TS_OA_NRT_OBSERVATIONS_013_002_a [WWW document]. Glob. Ocean. Real Time Situ Obs. Object. Anal. URL https://resources.marine.copernicus.eu/?option=com_csw&view=details&product_id=INSITU_GLO_TS_OA_NRT_OBSERVATIONS_013_002_a (accessed 7.26.20).

Girishkumar, M.S., Ravichandran, M., McPhaden, M.J., 2013. Temperature inversions and their influence on the mixed layer heat budget during the winters of 2006–2007 and 2007–2008 in the Bay of Bengal. J. Geophys. Res. Ocean 118, 2426–2437. http://dx.doi.org/10.1002/jgrc.20192.

Godfrey, J.S., Lindstrom, E.J., 1989. The heat budget of the equatorial western Pacific surface mixed layer. J. Geophys. Res. Ocean 94, 8007–8017. http://dx.doi.org/10.1029/JC094IC06P08007.

Gopalakrishna, V., Sadhuram, Y., Babu, V., 1988. Variability of Mixed Layer Depth in the Northern Indian Ocean During 1977 and 1979 Summer Monsoon Seasons. NISCAIR-CSIR.

Guinehut, S., Dhomps, A.L., Larnicol, G., Le Traon, P.Y., 2012. High resolution 3-D temperature and salinity fields derived from in situ and satellite observations. Ocean Sci. 8, 845–857. http://dx.doi.org/10.5194/os-8-845-2012.

Hacker, P., Firing, E., Hummon, J., Gordon, A.L., Kindle, J.C., 1998. Bay of Bengal currents during the northeast Monsoon. Geophys. Res. Lett. 25, 2769–2772. http://dx.doi.org/10.1029/98GL52115.

Jeandel, C., Thouron, D., Fieux, M., 1998. Concentrations and isotopic compositions of neodymium in the eastern Indian Ocean and Indonesian straits. Geochimica et Cosmochimica Acta 62 (15), 2597–2607. http://dx.doi.org/10.1016/S0016-7037(98)00169-0.

Kara, A.B., Rochford, P.A., Hurlburt, H.E., 2000. An optimal definition for ocean mixed layer depth. J. Geophys. Res. Ocean 105, 16803–16821. http://dx.doi.org/10.1029/2000jc900072.

Kara, A. Birol, Rochford, Peter A., Hurlburt, Harley E., Kara, A.B., Rochford, P.A., Hurlburt, H.E., 2003. Mixed layer depth variability over the global ocean. J. Geophys. Res. Ocean 108, 3079. http://dx.doi.org/10.1029/2000JC000736.

Kim, S.H., Choi, B.K., Kim, E., 2020. Study on the behavior of the water temperature inversion layer in the northern east China sea. J. Mar. Sci. Eng. 8, 157. http://dx.doi.org/10.3390/JMSE8030157, 2020, 8, 157.

Kumar, M.D., Li, Y.H., 1996. Spreading of water masses and regeneration of silica and 226Ra in the Indian ocean. Deep Sea Res. Part II Top. Stud. Oceanogr. 43, 83–110. http://dx.doi.org/10.1016/0967-0645(95)00084-4.

Kumari, A., Kumar, S.P., Chakraborty, A., 2018. Seasonal and interannual variability in the barrier layer of the Bay of Bengal. J. Geophys. Res. Ocean 123, 1001–1015. http://dx.doi.org/10.1002/2017JC013213.

Kurian, J., Vinayachandran, P.N., 2006. Formation mechanisms of temperature inversions in the southeastern Arabian sea. Geophys. Res. Lett. 33, 1–5. http://dx.doi.org/10.1029/2006GL027280.

Liao, J., Peng, S., Wen, X., 2020. On the heat budget and water mass exchange in the Andaman sea. Acta Oceanol. Sin. 39, 32–41. http://dx.doi.org/10.1007/S13131-019-1627-8, 2020 397.

Lukas, R., Lindstrom, E., 1991. The mixed layer of the western equatorial Pacific ocean. J. Geophys. Res. 96, 3343. http://dx.doi.org/10.1029/90jc01951.

Maes, C., O'Kane, T.J., 2014. Seasonal variations of the upper ocean salinity stratification in the tropics. J. Geophys. Res. Ocean 119, 1706–1722. http://dx.doi.org/10.1002/2013JC009366.

Masud-Ul-Alam, M., Khan, M.A.I., Barrett, B.S., Rivero-Calle, S., 2022. Surface temperature and salinity in the northern Bay of Bengal: in situ measurements compared with satellite observations and model output. J. Appl. Rem. Sens. 16, 018502. http://dx.doi.org/10.1117/1.JRS.16.018502.

Masud-Ul-Alam, Md., Khan, M.A.I., Islam, M.N., Rahman, S.M.M., 2020a. Modeling spatio-temporal variability of suspended matter and its relation with hydrodynamic parameters in the northern Bay of Bengal. Model. Earth Syst. Environ. 1–14. http://dx.doi.org/10.1007/s40808-020-01053-9.

Masud-Ul-Alam, Md., Khan, M.A.I., Sunny, S.K., Rahman, A., Rahman, M.S., Mahmud, B., Shaheen, A.R., 2020b. An exclusive in-situ dataset on physicochemical parameters in the gappy northern Bay of Bengal. Data Br. 31, 106024. http://dx.doi.org/10.1016/j.dib.2020.106024.

Mathew, S., Natesan, U., Latha, G., Venkatesan, R., Rao, R.R., Ravichandran, M., 2018. Observed warming of sea surface temperature in response to tropical cyclone Thane in the Bay of Bengal. Curr. Sci. 114, 1407–1413. http://dx.doi.org/10.18520/cs/v114/i07/1407-1413.

McCreary, J.P., Han, W., Shankar, D., Shetye, S.R., 1996. Dynamics of the east India coastal current: 2. Numerical solutions. J. Geophys. Res. Ocean 101, 13993–14010. http://dx.doi.org/10.1029/96JC00560.

McCreary, J.P., Kundu, P.K., Molinari, R.L., 1993. A numerical investigation of dynamics, thermodynamics and mixed-layer processes in the Indian ocean. Prog. Oceanogr. http://dx.doi.org/10.1016/0079-6611(93)90002-U.

Mili, M.I.J., Ahmed, M.K., Masud-Ul-Alam, M., Hasnain, M., Khan, M.A.I., Loodh, R., Abdullah-Al-Hasan, Belayet Hossain, K., Al Nahian, S., 2021. In-situ datasets of important physical and bio-chemical parameters in the continental shelf of the northern Bay of Bengal. Data Br. 35, 106947. http://dx.doi.org/10.1016/j.dib.2021.106947.

Murty, V.S.N., Sarma, Y.V.B., Rao, D.P., Murty, C.S., 1992. Water characteristics, mixing and circulation in the Bay of Bengal during southwest monsoon. J. Mar. Res. 50, 207–228. http://dx.doi.org/10.1357/002224092784797700.

Nagura, M., Terao, T., Hashizume, M., 2015. The role of temperature inversions in the generation of seasonal and interannual SST variability in the far northern Bay of Bengal. J. Clim. 28, 3671–3693. http://dx.doi.org/10.1175/JCLI-D-14-00553.1.

Nardelli, B., Droghei, R., Santoleri, R., 2016. Multi-dimensional interpolation of SMOS sea surface salinity with surface temperature and in situ salinity data. Rem. Sens. Environ. 180, 392–402. http://dx.doi.org/10.1016/j.rse.2015.12.052.

Narvekar, J., Prasanna Kumar, S., 2006. Seasonal variability of the mixed layer in the central Bay of Bengal and associated changes in nutrients and chlorophyll. Deep. Res. Part I Oceanogr. Res. Pap. 53, 820–835. http://dx.doi.org/10.1016/j.dsr.2006.01.012.

Narvekar, J., Prasanna Kumar, S., 2014. Mixed layer variability and chlorophyll-a biomass in the Bay of Bengal. Biogeosciences 11, 3819–3843. http://dx.doi.org/10.5194/bg-11-3819-2014.

Ning, J., Xu, Q., Zhang, H., Wang, T., Fan, K., 2019. Impact of cyclonic ocean eddies on upper ocean thermodynamic response to typhoon soudelor. Rem. Sens. 11, 938. http://dx.doi.org/10.3390/rs11080938.

Nyadjro, E.S., Subrahmanyam, B., Murty, V.S.N., Shriver, J.F., 2010. Salt transport in the near-surface layer in the monsoon-influenced Indian ocean using HYCOM. Geophys. Res. Lett. 37. http://dx.doi.org/10.1029/2010GL044127.

Pang, S., Wang, X., Liu, H., Zhou, G., Fan, K., 2019. Decadal variability of the barrier layer and forcing mechanism in the Bay of Bengal. J. Geophys. Res. Ocean 124, 5289–5307. http://dx.doi.org/10.1029/2018JC014918.

Potemra, J.T., 2005. Indonesian through flow transport variability estimated from satellite altimetry. Oceanography 18, 98–107. http://dx.doi.org/10.5670/OCEANOG.2005.10.

Prasad, T.G., 1997. Annual and seasonal mean buoyancy fluxes for the tropical Indian ocean. Curr. Sci. http://dx.doi.org/10.2307/24100427.

Prasanna Kumar, S., 2004. Intrusion of the Bay of Bengal water into the arabian sea during winter monsoon and associated chemical and biological response. Geophys. Res. Lett. 31, L15304. http://dx.doi.org/10.1029/2004GL020247.

Raju, D.V., Gouveia, A.D., Murty, C.S., 1981. Some physical characteristics of Andaman sea waters during winter. Indian J. Geo-Mar. Sci. 10, 211–218.

Rao, D.P., Sarma, V.V., Rao, V.S., Sudhakar, U., Gupta, G.V.M., 1996. On watermass mixing ratios and regenerated silicon in the Bay of Bengal. Indian J. Geo-Mar. Sci. 25, 56–61.

Reynolds, R.W., Rayner, N.A., Smith, T.M., Stokes, D.C., 2002. An improved in situ and satellite SST analysis for climate. In: Journal of Climate. American Meteorological Society, http://dx.doi.org/10.1175/1520-0442(2002)015<1609:AIISAS>2.0.CO;2.

Rio, M.H., Mulet, S., 2014. Beyond GOCE for the ocean circulation estimate: Synergetic use of altimetry, gravimetry, and in situ data provides new insight into geostrophic and Ekman currents. Geophysical Research Letters 41 (14), 8918–8925, 10.1002/2014GL061773@10.1002/(ISSN)1944-8007.GRLEDITORHGHLTS2014.

Rudnick, D.L., Ferrari, R., 1999. Compensation of horizontal temperature and salinity gradients in the ocean mixed layer. Science 283, 526–529. http://dx.doi.org/10.1126/SCIENCE.283.5401.526.

Sardessai, S., Ramaiah, N., Prasanna Kumar, S., de Sousa, S.N., 2007. Influence of environmental forcings on the seasonality of dissolved oxygen and nutrients in the Bay of Bengal. J. Mar. Res. 65, 301–316. http://dx.doi.org/10.1357/002224007780882578.

Sengupta, S., Parekh, A., Chakraborty, S., Ravi Kumar, K., Bose, T., 2013. Vertical variation of oxygen isotope in Bay of Bengal and its relationships with water masses. J. Geophys. Res. 118, 6411–6424. http://dx.doi.org/10.1002/2013JC008973.

Shankar, D., 2004. Observational evidence for westward propagation of temperature inversions in the southeastern Arabian sea. Geophys. Res. Lett. 31, L08305. http://dx.doi.org/10.1029/2004GL019652.

Shankar, D., Gopalakrishna, V.V., Shenoi, S.S.C., Durand, F., Shetye, S.R., Rajan, C.K., Johnson, Z., Araligidad, N., Michael, G.S., 2004. Observational evidence for westward propagation of temperature inversions in the southeastern Arabian sea. Geophys. Res. Lett. 31. http://dx.doi.org/10.1029/2004GL019652.

Shankar, D., Vinayachandran, P.N., Unnikrishnan, A.S., 2002. The monsoon currents in the north Indian ocean. Prog. Oceanogr. http://dx.doi.org/10.1016/S0079-6611(02)00024-1.

Shenoi, S.S.C., Shankar, D., Shetye, S.R., 2002. Differences in heat budgets of the near-surface Arabian sea and Bay of Bengal: Implications for the summer monsoon. J. Geophys. Res. Ocean 107 (C6), http://dx.doi.org/10.1029/2000JC000679, 5–1.

Siddique, A., Bhowal, A., Purushothaman, J., Madhusoodhanan, R., Raghunathan, C., Chandra, K., 2021. Seasonal oceanographic phenomenon promotes hitchhiking among the plankton in a coastal marine ecosystem: A tropical perspective. Ecol. Indic. 129, 107914. http://dx.doi.org/10.1016/J.ECOLIND.2021.107914.

Singh, S.P., Singh, S.K., Goswami, V., Bhushan, R., Rai, V.K., 2012. Spatial distribution of dissolved neodymium and εNd in the Bay of Bengal: Role of particulate matter and mixing of water masses. Geochim. Cosmochim. Acta 94, 38–56. http://dx.doi.org/10.1016/J.GCA.2012.07.017.

Sprintall, J., Tomczak, M., 1992. Evidence of the barrier layer in the surface layer of the tropics. J. Geophys. Res. 97, 7305. http://dx.doi.org/10.1029/92jc00407.

Subramanian, V., 1993. Sediment load of Indian rivers. Curr. Sci. http://dx.doi.org/10.2307/24096213.

Thadathil, P., Gopalakrishna, V.V., Muraleedharan, P.M., Reddy, G.V., Araligidad, N., Shenoy, S., 2002. Surface layer temperature inversion in the Bay of Bengal. Deep. Res. Part I Oceanogr. Res. Pap. 49, 1801–1818. http://dx.doi.org/10.1016/S0967-0637(02)00044-4.

Thadathil, P., Gosh, A.K., 1992. Surface layer temperature inversion in the Arabian sea during winter. J. Oceanogr. 48, 293–304. http://dx.doi.org/10.1007/BF02233989.

Thadathil, P., Muraleedharan, P.M., Rao, R.R., Somayajulu, Y.K., Reddy, G.V., Revichandran, C., 2007. Observed seasonal variability of barrier layer in the Bay of Bengal. J. Geophys. Res. Ocean 112. http://dx.doi.org/10.1029/2006JC003651.

Thadathil, P., Suresh, I., Gautham, S., Prasanna Kumar, S., Lengaigne, M., Rao, R.R., Neetu, S., Hegde, A., 2016. Surface layer temperature inversion in the Bay of Bengal: Main characteristics and related mechanisms. J. Geophys. Res. Ocean 121, 5682–5696. http://dx.doi.org/10.1002/2016JC011674.

Thadathil, P., Thoppil, P., Rao, R.R., Muraleedharan, P.M., Somayajulu, Y.K., Gopalakrishna, V.V., Murthugudde, R., Reddy, G.V., Revichandran, C., 2008. Seasonal variability of the observed barrier layer in the Arabian sea. J. Phys. Oceanogr. 38, 624–638. http://dx.doi.org/10.1175/2007JPO3798.1.

Thangaprakash, V.P., Girishkumar, M.S., Suprit, K., Kumar, N.S., Chaudhuri, D., Dinesh, K., Kumar, A., Shivaprasad, S., Ravichandran, M., Farrar, J.T., Sundar, R., Weller, R.A., 2016. What controls seasonal evolution of sea surface temperature in the Bay of Bengal?: Mixed layer heat budget analysis using moored buoy observations along 90 °E. Oceanography 29, 202–213.

Thompson, B., Gnanaseelan, C., Salvekar, P.S., 2006. Seasonal evolution of temperature inversions in the north Indian ocean. Curr. Sci. http://dx.doi.org/10.2307/24089118.

Tomczak, M., Godfrey, J.S., 2003. Regional Oceanography: An Introduction. Daya books.

Trott, C.B., Subrahmanyam, B., Nyadjro, E.S., 2019. Influence of mesoscale features on mixed layer dynamics in the Arabian sea. J. Geophys. Res. Ocean 124, 3361–3377. http://dx.doi.org/10.1029/2019JC014965.

Ueno, H., Yasuda, I., 2003. Intermediate water circulation in the north Pacific subarctic and northern subtropical regions. J. Geophys. Res. Ocean 108. http://dx.doi.org/10.1029/2002jc001372.

Vinayachandran, P.N., Murty, V.S.N., Babu, V.R., 2002. Observations of barrier layer formation in the Bay of Bengal during summer monsoon. J. Geophys. Res. Ocean 107, SRF 19–1. http://dx.doi.org/10.1029/2001JC000831@10.1002/(ISSN)2169-9291.SURFSL1.

Vinayachandran, P.N., Shetye, S.R., Sengupta, D., Gadgil, S., 1996. Forcing mechanisms of the Bay of Bengal circulation. Curr. Sci. 71, 753–763.

Wang, J.W., Han, W., Sriver, R.L., 2012. Impact of tropical cyclones on the ocean heat budget in the Bay of Bengal during 1999: 2. Processes and interpretations. J. Geophys. Res. Ocean 117. http://dx.doi.org/10.1029/2012JC008373.

Weller, R.A., Plueddemann, A.J., 1996. Observations of the vertical structure of the oceanic boundary layer. J. Geophys. Res. Ocean 101, 8789–8806. http://dx.doi.org/10.1029/96JC00206.

You, Y., 1997. Seasonal variations of thermocline circulation and ventilation in the Indian ocean. J. Geophys. Res. Ocean 102, 10391–10422. http://dx.doi.org/10.1029/96JC03600.

You, Y., 2000. Implications of the deep circulation and ventilation of the Indian ocean on the renewal mechanism of north Atlantic deep water. J. Geophys. Res. Ocean 105, 23895–23926. http://dx.doi.org/10.1029/2000JC900105.

Yuan, D., Li, Y., He, L., Zhou, H., Li, R., Wang, F., Lei, H., Hu, D., 2010. An observation of the three-dimensional structure of a cross-shelf penetrating front off the Changjiang mouth. Deep. Res. Part II Top. Stud. Oceanogr. 57, 1827–1834. http://dx.doi.org/10.1016/j.dsr2.2010.04.009.